HRMAS Applications

Raffaele Lamanna[a]

[a]ENEA, Research Center Trisaia.

HRMAS Workshop Parma 31 Marzo 2014

Sistemi eterogenei

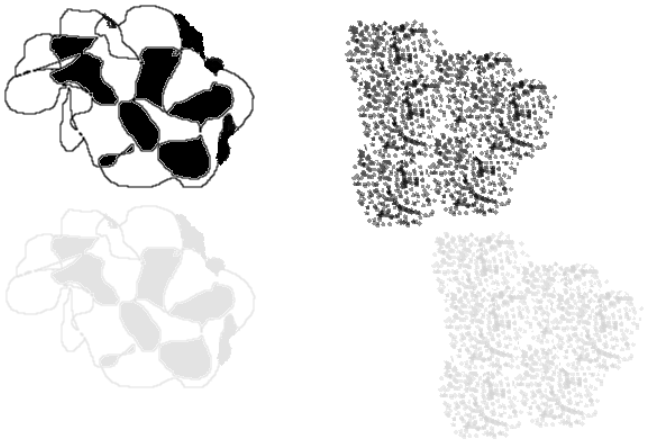

- composizione
- fase chimica
- fase fisica
- geometria

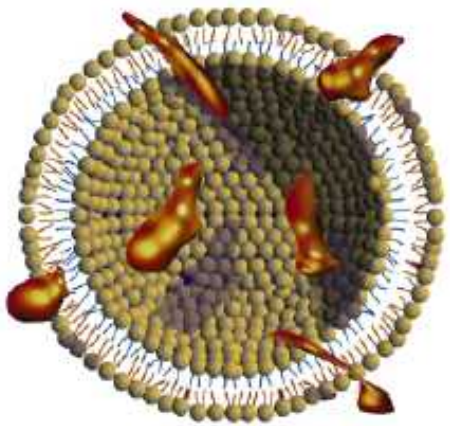

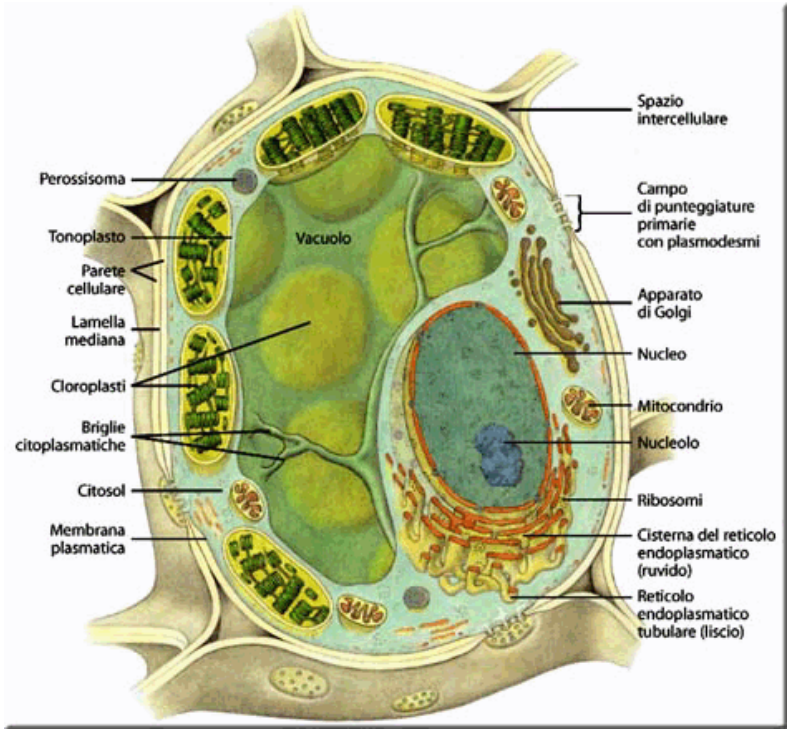

Identificazione di carotoidi in vegetali

MAGNETIC RESONANCE IN CHEMISTRY
Magn. Reson. Chem. 2006; **44**: 675–685
Published online 27 April 2006 in Wiley InterScience (www.interscience.wiley.com). DOI: 10.1002/mrc.1826

MRC

^{1}H HR-MAS NMR of carotenoids in aqueous samples and raw vegetables

M. L. Miglietta* and R. Lamanna

BIOTEC-AGRO ENEA C.R. Trisaia, S.S. 106 Jonica Km 419,500, 75026 Rotondella (Mt), Italy

Difficoltá di rivelazione in matrice

- Bassa concentrazione
- Eterogeneitá del campione
- Posizione ignota delle risonanze in ambiente eterogeneo
- Difficoltá di aggiunta di carotene al campione per elevato contenuto d'acqua

- Necessitá di studiare sistemi modello

Carotene in matrice polisaccaridica

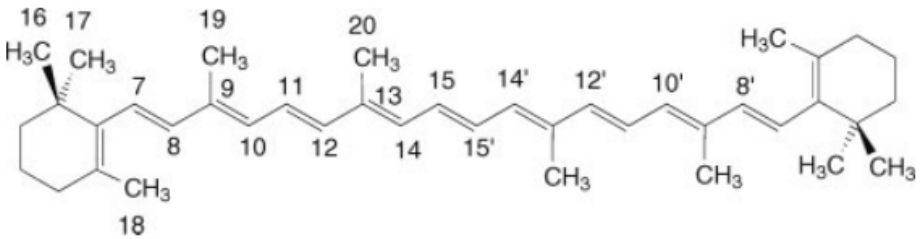

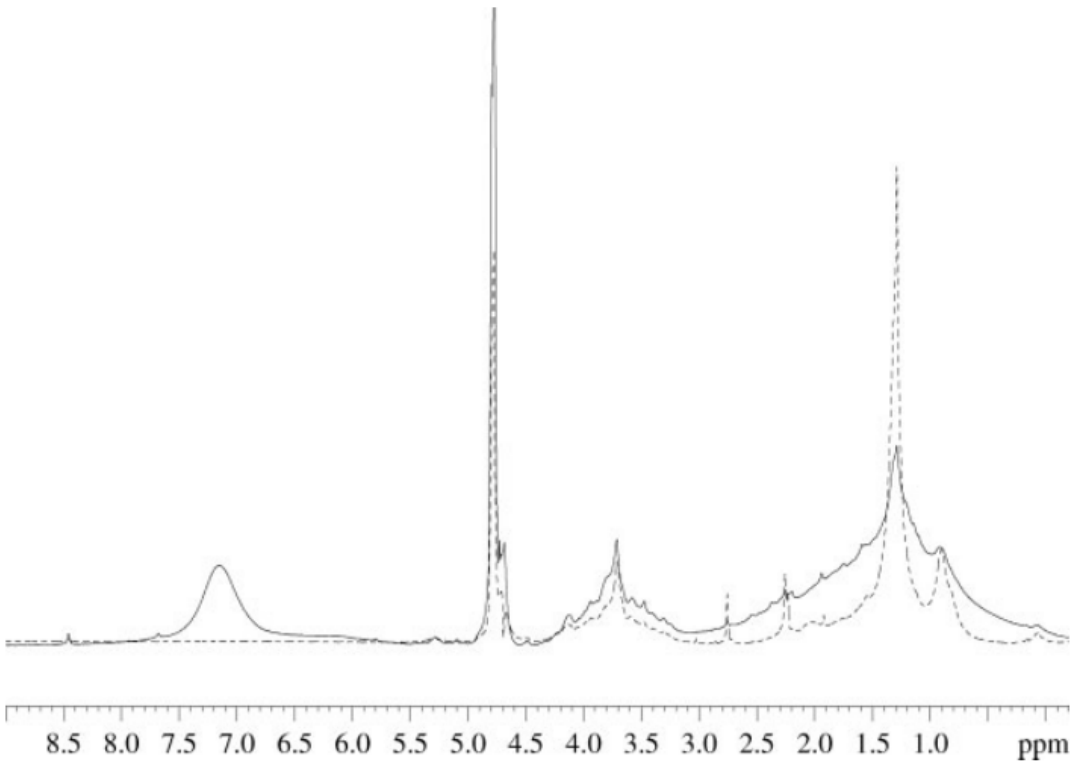

Figure 4. ^{1}H HR-MAS NMR spectrum of β-carotene adsorbed on the polysaccharidic matrix with D_2O (solid line) compared with the spectrum of the polysaccharidic matrix itself (dashed line). The β-carotene olefinic protons are clearly visible as a broad signal at 7.15 ppm.

Carotene+lipidi+acqua

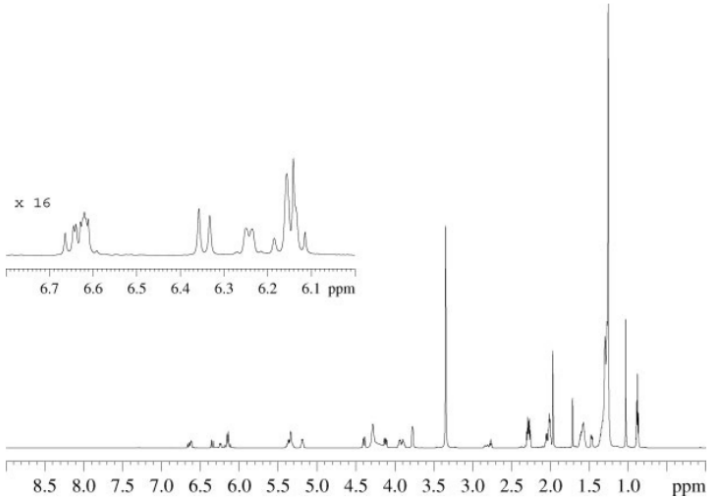

Figure 5. ^{1}H NMR spectrum of the starting chloroform mixture of β-carotene and EYPC (1 : 3 molar ratio) used to prepare the MLVs containing β-carotene. The inset shows the characteristic olefinic protons of β-carotene.

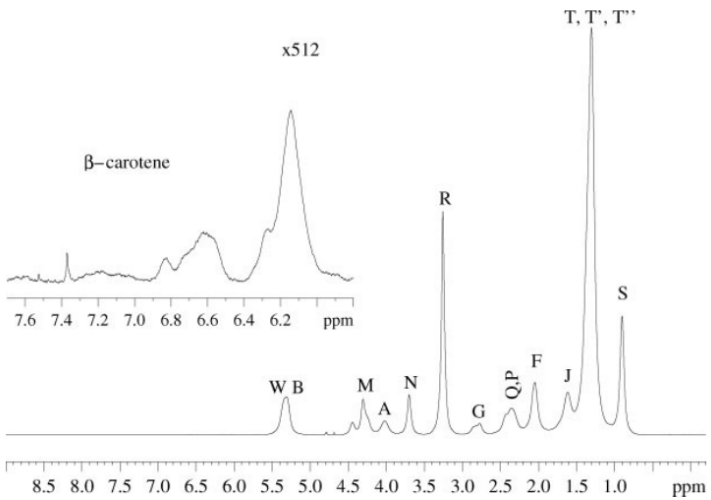

Figure 6. ^{1}H HR-MAS NMR spectrum of MLVs of EYPC containing β-carotene (27 mol%) in D_2O buffer solution, with some assignments of EYPC resonances (labels are referred to the chemical structure **2**). The inset shows the resonances of β-carotene molecules embedded in the MLV system on an enlarged vertical scale. The very broad β-carotene resonances are detected at 6.14, 6.27, 6.61 and 6.83 ppm.

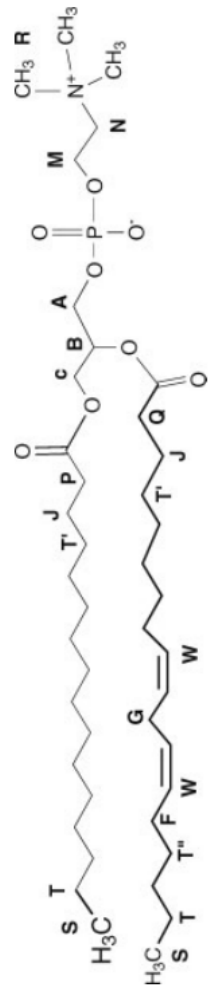

Solo 1% del β-carotene totale é visibile nel liposoma.

Carotene+lipidi+polisaccaridi+acqua

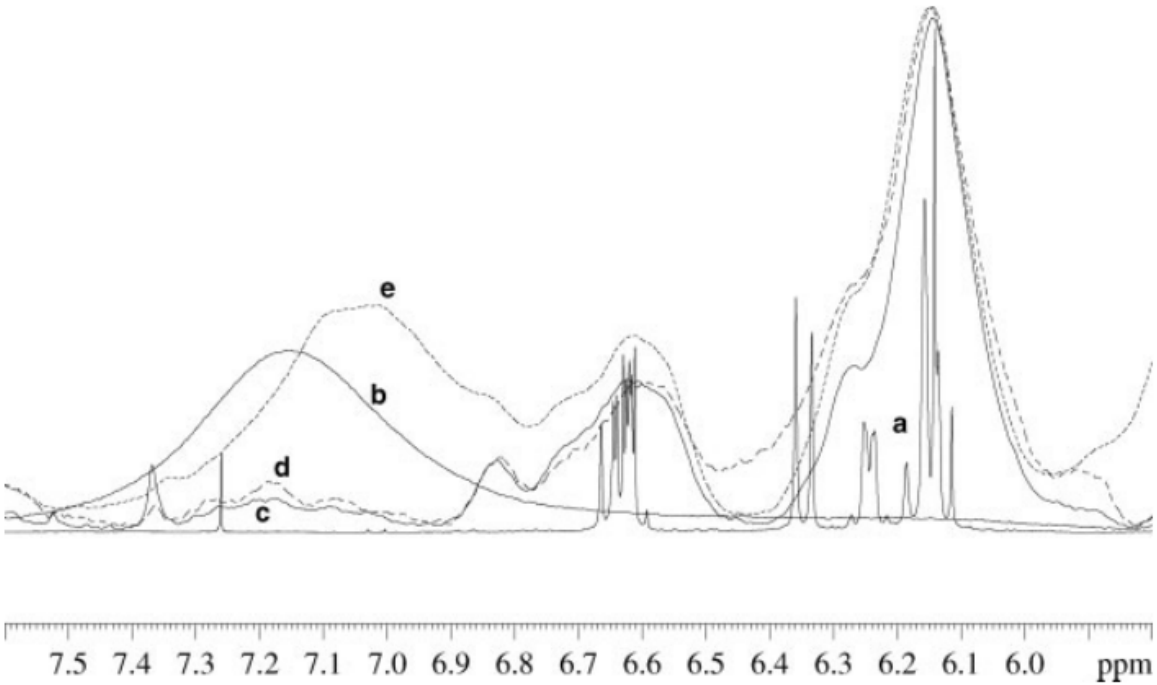

Figure 7. Comparison among ^{1}H HR-MAS NMR spectra of the olefinic protons of β-carotene in the model samples: (a) β-carotene in $CDCl_3$ solution; (b) β-carotene in the polysaccharidic matrix with D_2O; (c) β-carotene resonances in MLVs (D_2O, buffer solution); (d) MLVs on the polysaccharidic matrix; (e) β-carotene/EYPC mixture (1 : 3 molar ratio) adsorbed on the polysaccharidic matrix with D_2O.

Natural carotene-lipid extract

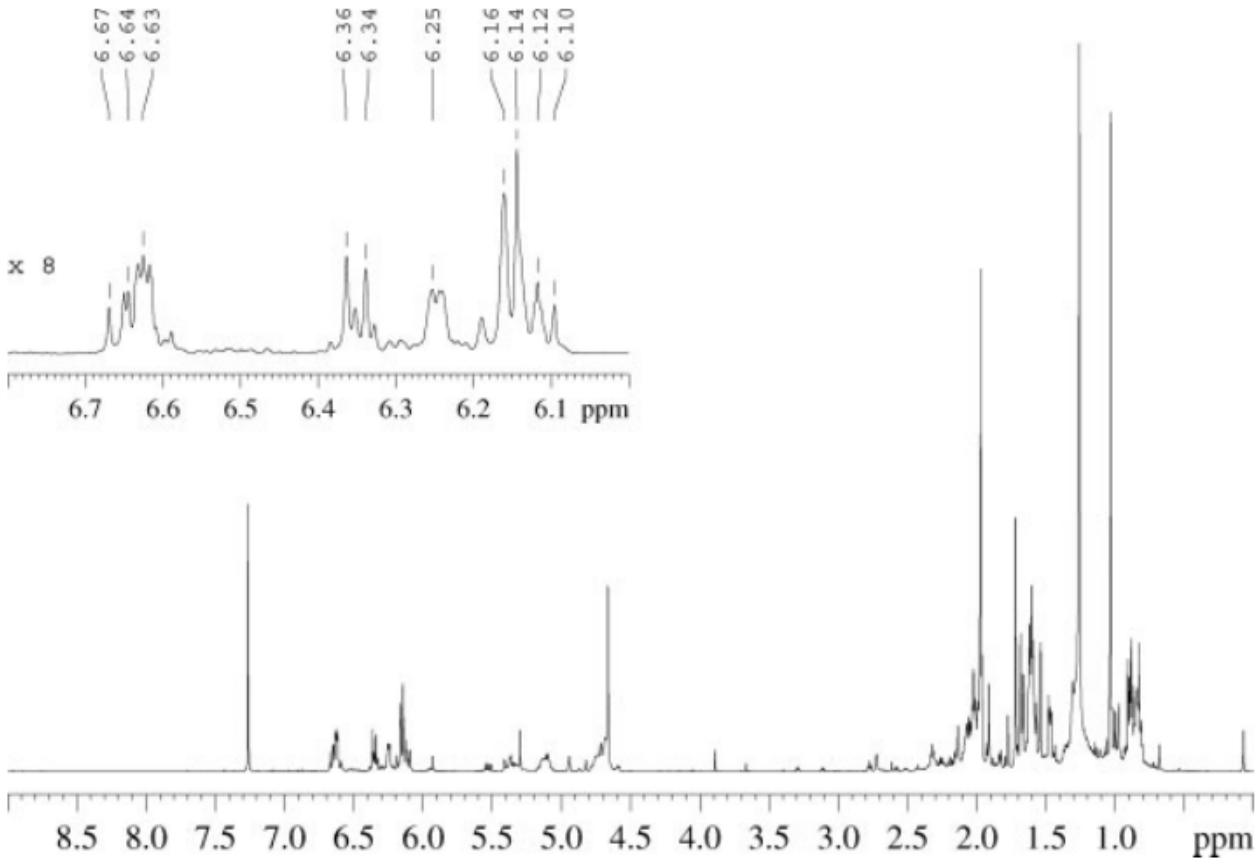

Figure 8. ^{1}H NMR spectrum of carotenoid extracts in $CDCl_3$. The inset shows the olefinic proton signals of carotenoids.

natural carotene of saccharidic matrix

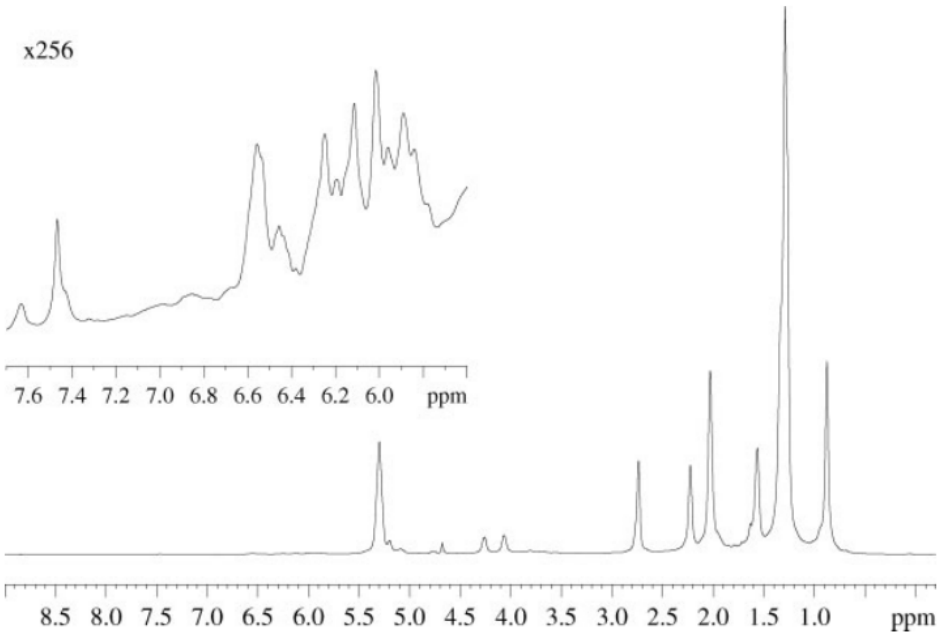

Figure 9. ^{1}H HR-MAS NMR spectrum of carotenoid extracts adsorbed on the polysaccharidic matrix with D_2O. The inset shows the expansion of the carotenoids resonances.

natural carotene + natural solid model

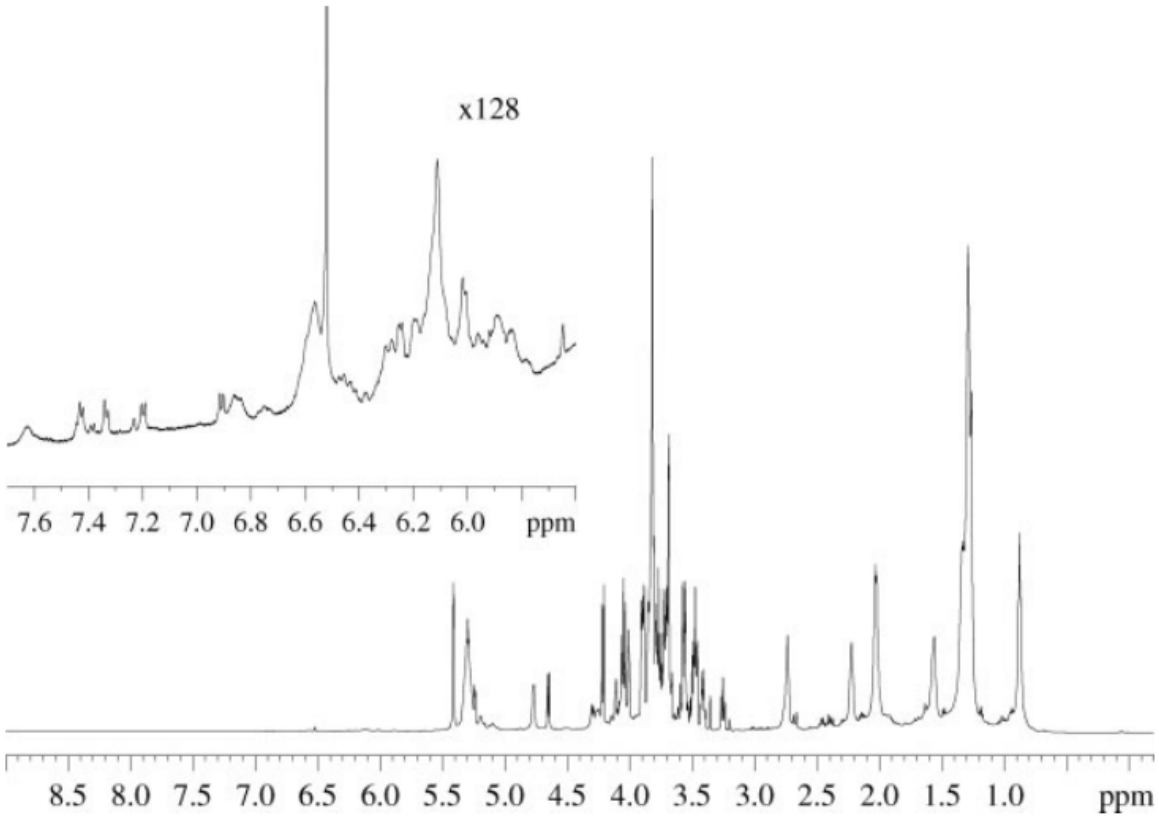

Figure 10. ^{1}H HR-MAS NMR spectrum of the vegetable matrix samples with the addition of the carotenoid extract. In the inset, the olefinic region with an expanded vertical scale is shown.

Confronto modelli

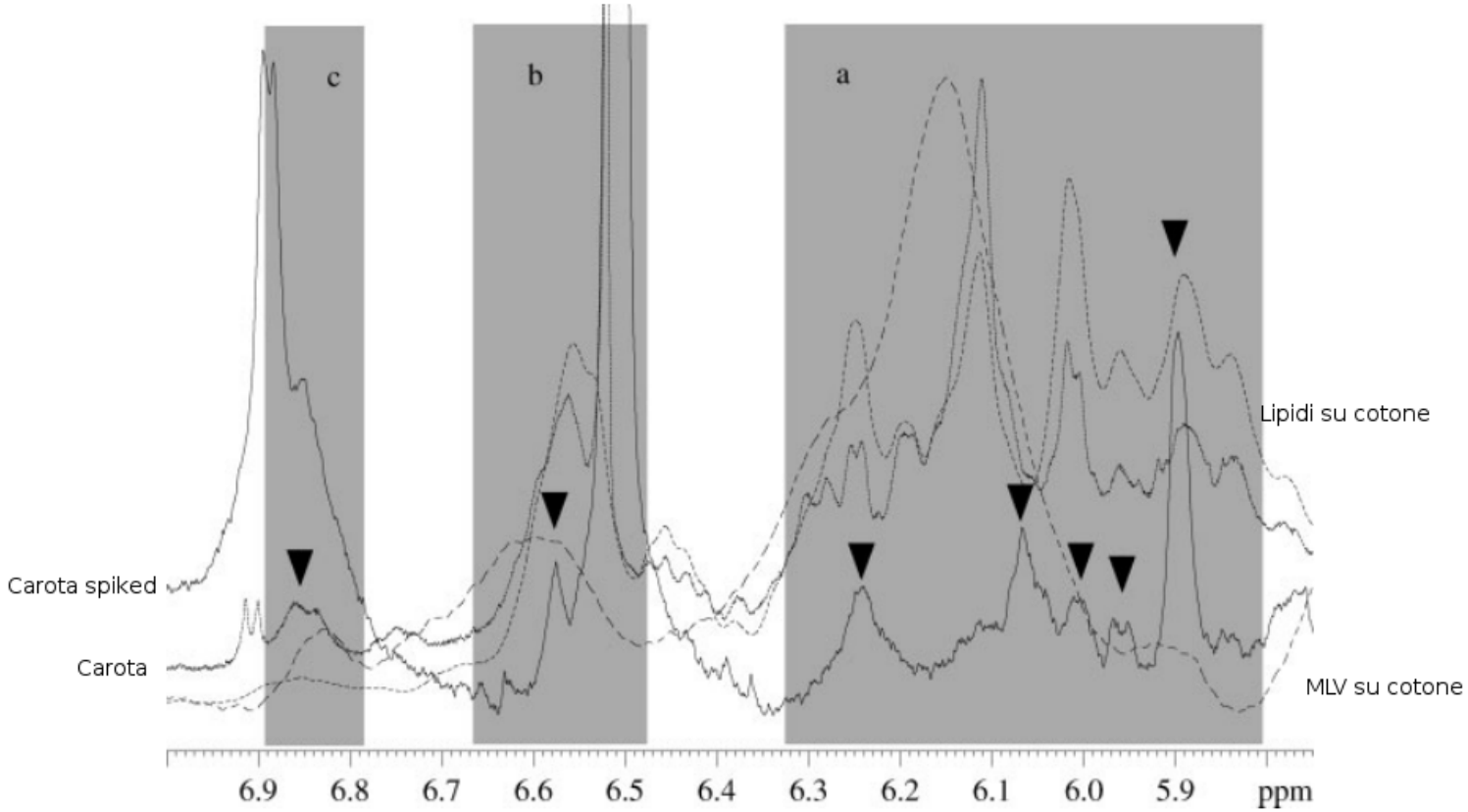

Figure 11. Comparison among ^{1}H HR-MAS spectra of the three-phase model systems with the raw vegetable matrix spectrum (solid line) in the olefinic region: β-carotene embedded in liposomes adsorbed on cotton wool (dashed line); cotton sample soaked with a lipid–carotenoid extract (short dashed line); lyophilized carrot sample with lipid–carotenoid extract (dotted line). Arrows indicate the signals of the raw carrot sample that can be attributed to carotenoids resonances according to the spectra of the model systems. The vertical expansion of each spectrum is adjusted to reduce the superposition of the curves in order to improve readability.

Molecole chirali in liposomi

ELSEVIER

Available online at www.sciencedirect.com
ScienceDirect
Tetrahedron: *Asymmetry* 17 (2006) 2731–2737

Tetrahedron: *Asymmetry*

Chiral recognition of dipeptides in phosphatidylcholine aggregates

Oscar Cruciani,[a,b] Stefano Borocci,[c] Raffaele Lamanna,[d] Giovanna Mancini[a,b,e,*] and Anna Laura Segre[a]

[a]*Istituto di Metodologie Chimiche-IMC, C.N.R., Area della Ricerca di Roma. C.P. 10, 00016 Monterotondo Stazione Roma, Italy*
[b]*Dipartimento di Chimica, Università degli Studi di Roma 'La Sapienza', P.le A. Moro 5. 00185 Roma, Italy*
[c]*Dipartimento di Scienze Ambientali, Università degli Studi della Tuscia, P.le dell'Università, 01100 Viterbo, Italy*
[d]*CR ENEA Trisaia UTS Biotec-Agro SS 106 Jonica Km 419.5, 75026 Rotondella (Mt), Italy*
[e]*Centro di Eccellenza Materiali Innovativi Nanostrutturati per Applicazioni Chimiche Fisiche e Biomediche, Italy*

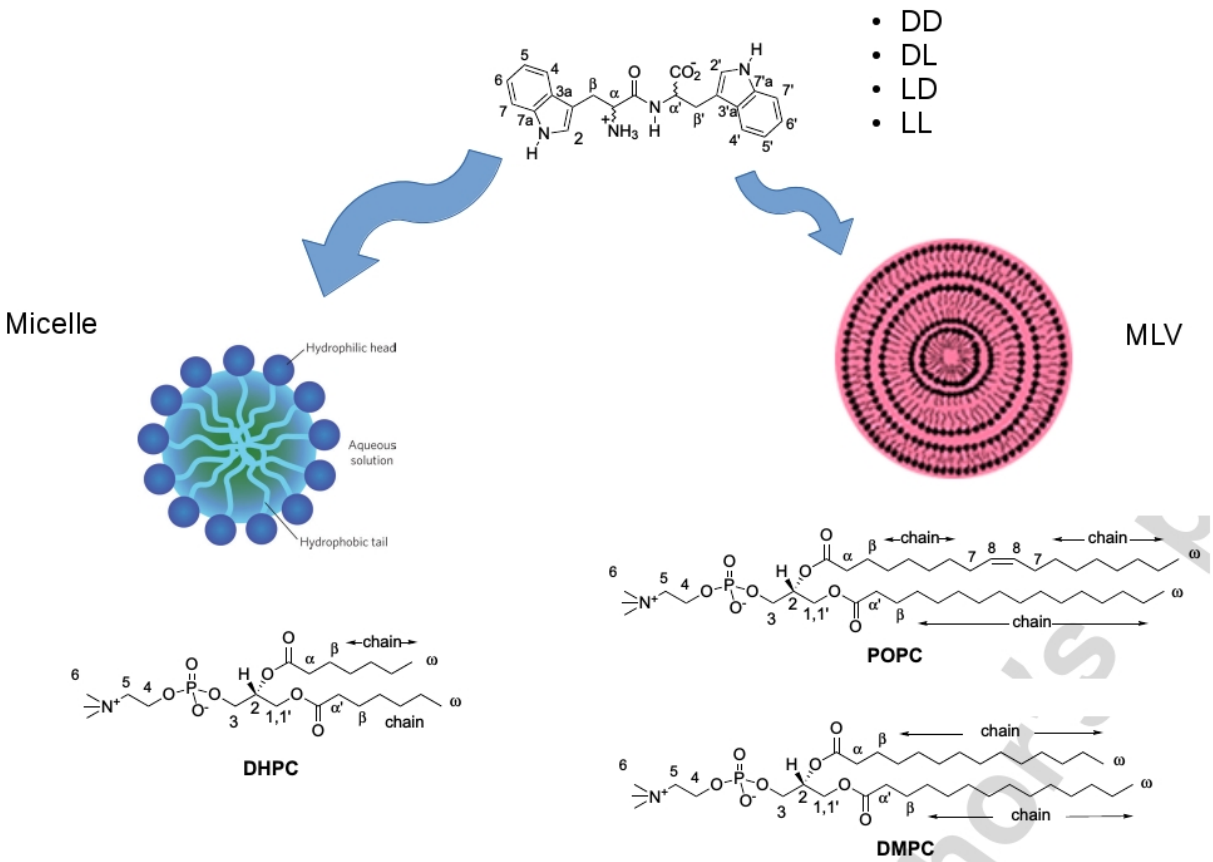

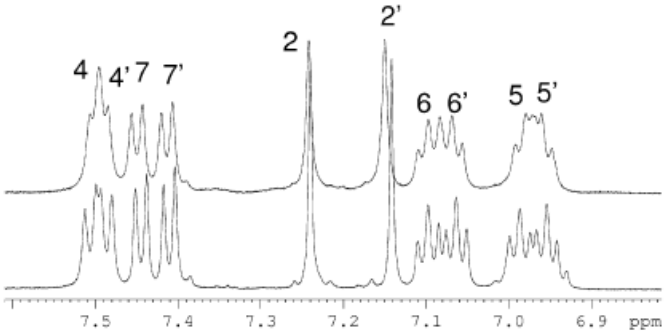

Figure 1. Comparison of the aromatic region of the 600.13 MHz ^{1}H NMR spectra of 5 mM **1** homochiral enantiomers in 50 mM DHPC (DD-**1** top, LL-**1** down). The spectra were obtained in an aqueous buffered solution (100 mM phosphate buffer, pD = 5.8) at 300 K.

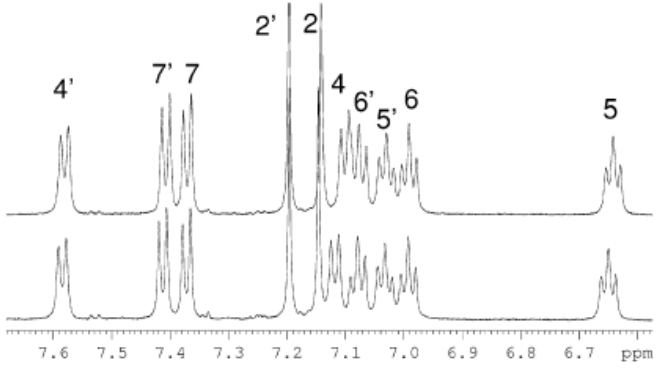

Figure 2. Comparison of the aromatic region of the 600.13 MHz ^{1}H NMR spectra of 5 mM **1** heterochiral enantiomers in 50 mM DHPC (LD-**1** top, DL-**1** down). The spectra were obtained in an aqueous buffered solution (100 mM phosphate buffer, pD = 5.8) at 300 K.

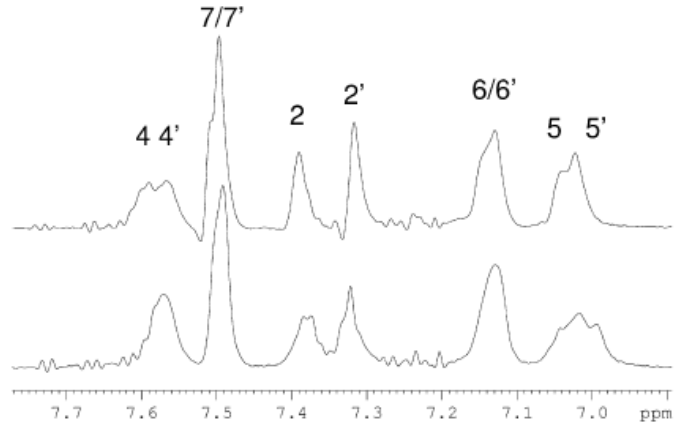

Figure 3. Comparison of the aromatic region of the 600.13 MHz ^{1}H HR-MAS spectra of 36 mM **1** homochiral enantiomers in the aqueous multilamellar dispersion of POPC (LL-**1** top, DD-**1** down). The spectra were obtained in an aqueous buffered solution (100 mM phosphate buffer, pD = 5.8) and performed at 10 kHz, setting the temperature at 300 K.

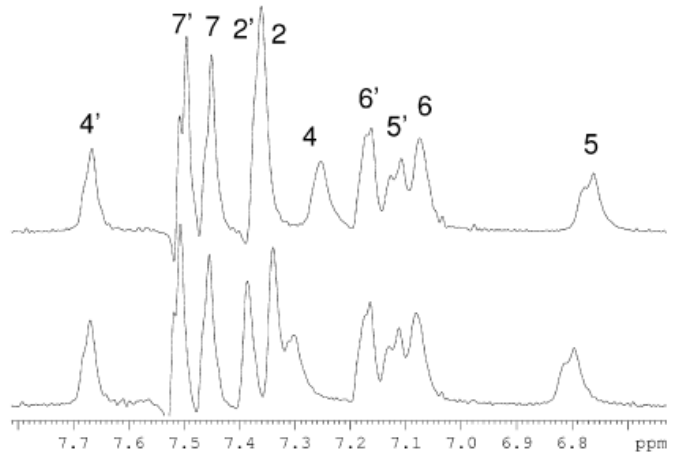

Figure 4. Comparison of the aromatic region of the 600.13 MHz ^{1}H HR-MAS spectra of 36 mM **1** heterochiral enantiomers in the aqueous multilamellar dispersion of POPC (LD-**1** top, DL-**1** down). The spectra were obtained in an aqueous buffered solution (100 mM phosphate buffer, pD = 5.8) and performed at 10 kHz, setting the temperature at 300 K.

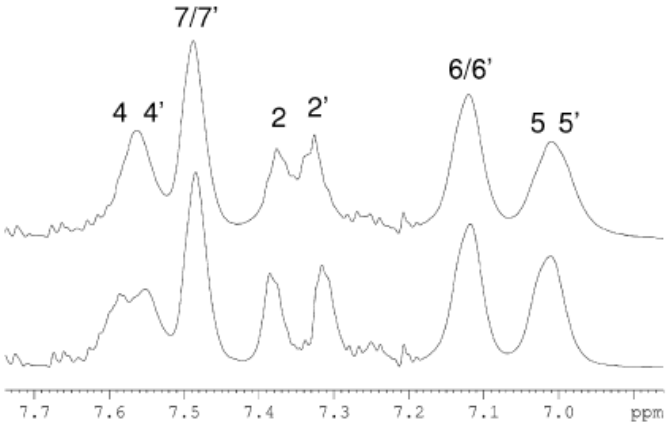

Figure 5. Comparison of the aromatic region of the 600.13 MHz ^{1}H HR-MAS spectra of 36 mM **1** homochiral enantiomers in the aqueous multilamellar dispersion of DMPC (LL-**1** down, DD-**1** top). The spectra were obtained in an aqueous buffered solution (100 mM phosphate buffer, pD = 5.8) and performed at 10 kHz, setting the temperature at 300 K.

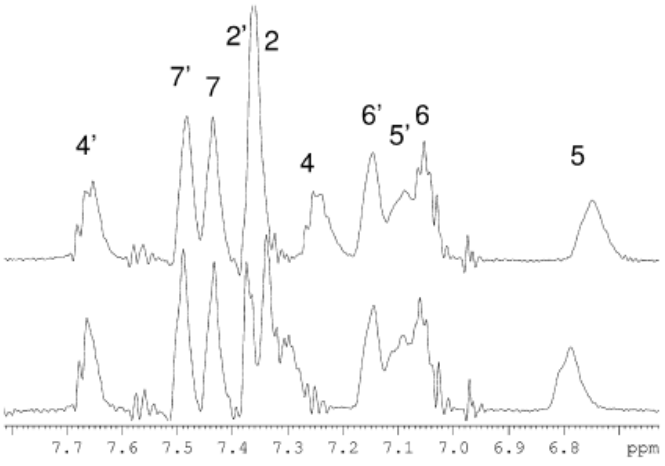

Figure 6. Comparison of the aromatic region of the 600.13 MHz ^{1}H HR-MAS spectra of 36 mM **1** heterochiral enantiomers in aqueous multilamellar dispersion of DMPC (LD-**1** top, DL-**1** down). The spectra were obtained in an aqueous buffered solution (100 mM phosphate buffer, pD = 5.8) and performed at 10 kHz, setting the temperature at 300 K.

1. L'interazione diastereomerica fra il peptide e gli aggregati produce differenti shift per i diversi enantiomeri del ditriptofano.
2. La stessa coppia di enantiomeri é discriminata in maniera diversa dai differenti tipi di aggregati.

Effetti del peptide sui segnali lipidici

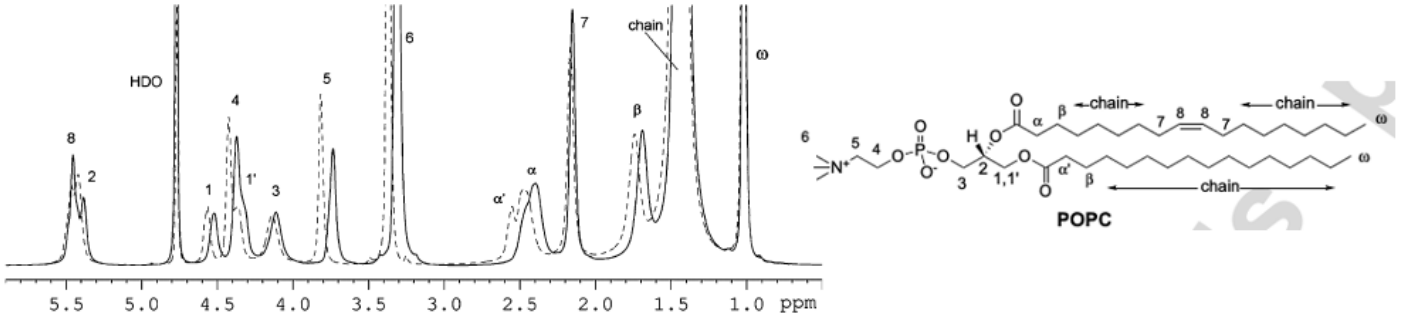

Figure 7. Comparison of the 600.13 MHz ^{1}H HR-MAS NMR (10 kHz) spectra of the aqueous multilamellar dispersion of POPC in the absence (grey dashed trace) and in the presence of **DD-1** (black trace).

Table 2. Chemical shift variations of the signals due to the aggregates in the presence of dipeptides

Type	LL-1			DD-1			DL-1			LD-1		
	POPC	DMPC	DHPC	POPC	DMPC	DHPC	POPC	DMPC	DHPC	POPC	DMPC	DHPC
ωCH_3	6	0	10	6	0	11	0	0	13	0	0	13
Chain	6	6	19	6	6	17	6	6	20	6	6	20
α	42	36	28	36	30	28	24	30	27	30	30	26
α′	42	48	26	54	54	26	36	54	27	42	48	28
β	30	30	25	24	24	24	24	24	24	24	24	24
1	18	18	15	18	24	16	12	12	11	12	12	10
1′	24	18	14	30	12	13	12	12	8	12	12	9
2	18	18	9	18	12	10	6	6	4	6	6	4
3	12	18	8	12	12	8	0	6	3	0	6	2
4	30	24	25	36	24	25	24	18	19	24	18	19
5	48	42	41	54	42	41	36	36	35	36	36	35
6	36	36	30	42	30	29	30	30	26	30	30	26
7	12	—	—	12	—	—	12	—	—	6	—	—
8	6	—	—	12	—	—	6	—	—	6	—	—

Table 2. Chemical shift variations of the signals due to the aggregates in the presence of dipeptides

Type	LL-1			DD-1			DL-1			LD-1		
	POPC	DMPC	DHPC	POPC	DMPC	DHPC	POPC	DMPC	DHPC	POPC	DMPC	DHPC
ωCH_3	6	0	10	6	0	11	0	0	13	0	0	13
Chain	6	6	19	6	6	17	6	6	20	6	6	20
α	42	36	28	36	30	28	24	30	27	30	30	26
α′	42	48	26	54	54	26	36	54	27	42	48	28
β	30	30	25	24	24	24	24	24	24	24	24	24
1	18	18	15	18	24	16	12	12	11	12	12	10
1′	24	18	14	30	12	13	12	12	8	12	12	9
2	18	18	9	18	12	10	6	6	4	6	6	4
3	12	18	8	12	12	8	0	6	3	0	6	2
4	30	24	25	36	24	25	24	18	19	24	18	19
5	48	42	41	54	42	41	36	36	35	36	36	35
6	36	36	30	42	30	29	30	30	26	30	30	26
7	12	—	—	12	—	—	12	—	—	6	—	—
8	6	—	—	12	—	—	6	—	—	6	—	—

- Gli stereoisomeri si posizionano vicino alla testa del fosfolipide indipendentemente dalla curvatura superficiale o dall'organizzazione degli aggregati.
- L'iterazione di ciascun stereoisomero con l'aggregato lipidico é funzione del tipo di aggregato
- Il riconoscimento chirale coinvolge un ampia regione dell'aggregato piuttosto che l'interazione col centro chirale di un singolo monomero.
- Il riconoscimento chirale in micelle e liposomi é frutto di una serie complessa di meccanismi.

Dipeptide conformation

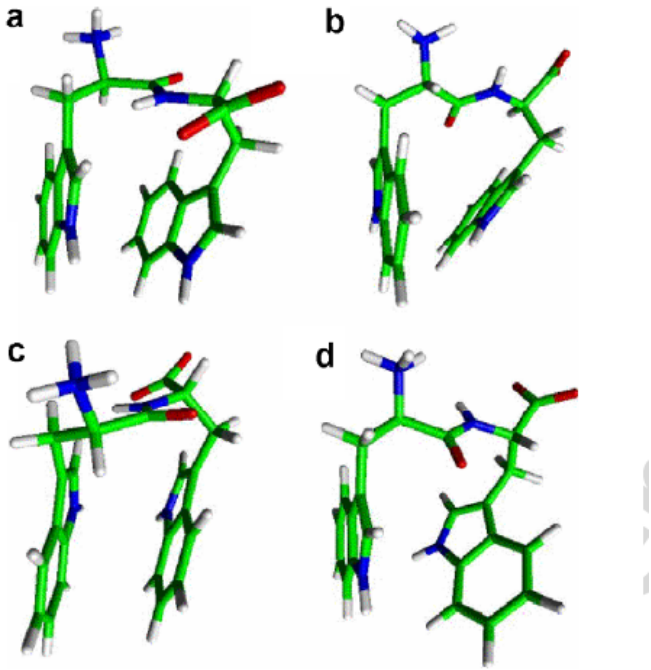

Figure 8. Stick representation of the minimum energy conformer, obtained by a restrained conformational search, of (a) DD-1 in POPC, (b) LD-1 in POPC, (c) LL-1 in POPC, (d) DL-1 in POPC.

- Le conformazioni sono simili in DHPC, POPC e DMPC

Hydrogels

*"Hydrogels are three-dimensional, hydrophilic, polymeric networks capable of imbibing large amounts of water or biological fluids"**

A three-dimensional crosslinked network that swells in an aqueous medium without dissolving ⇨

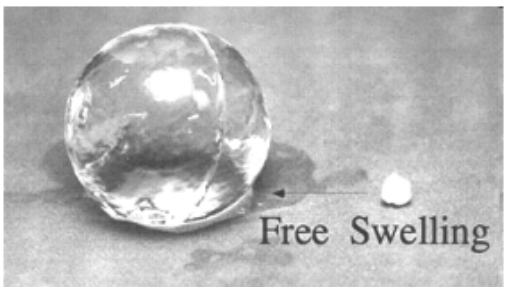

Cross-link formation

I meccanismi di formazione dei cross-link e la loro distribuzione sulla catena sono fondamentali per il funzionamento.

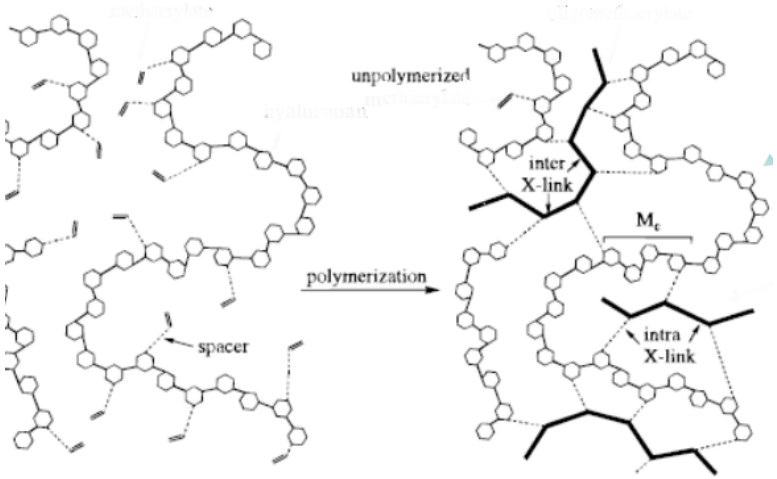

Hydrogel network structures

Chemical hydrogels → covalent crosslinks

Physical hydrogels → physical crosslinks → ionic interactions; hydrogen bonds; Van der Waals forces; ...

Cross link determination in ClickGel reactions

Biomacromolecules **2007,** *8,* *1844−1850*

Novel Hydrogels via Click Chemistry: Synthesis and Potential Biomedical Applications

Vittorio Crescenzi,*,† Lisa Cornelio,† Chiara Di Meo,† Stefania Nardecchia,† and Raffaele Lamanna‡

Department of Chemistry, University of Rome Sapienza, P.le Aldo Moro 5, 00185 Rome, Italy and Department BAS, CR ENEA Trisaia, ss 106 jonica Km 419.5, 75026 Rotondella (Mt), Italy

Scheme 3. Schematic Representation of the Formation of HA-Based Click-Gels

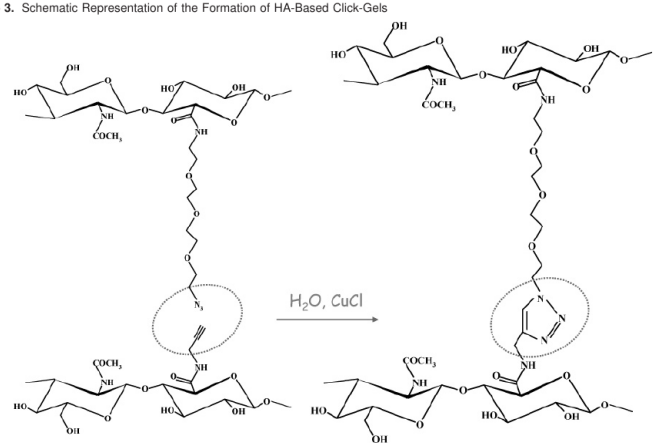

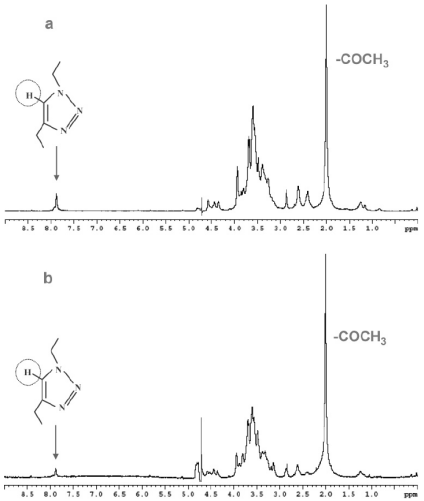

Figure 1. ^{1}H HR-MAS NMR (600.13 MHz) spectra of click-gel CG-1 (a) and click-gel CG-2 (b). The resonances used for the semiquantitative analysis are indicated, i.e., the triazole ring proton and acetyl protons.

$$CD = \frac{I(T)}{\left(\frac{I(A)}{3}\right)} \times 100$$

$CD_a = 21\%$

$CD_b = 8\%$

ClickGel

Influence of dialkyne structure on the properties of new click-gels based on hyaluronic acid

Gabriella Testa[a], Chiara Di Meo[a,1], Stefania Nardecchia[a], Donatella Capitani[b], Luisa Mannina[c,b], Raffaele Lamanna[d], Andrea Barbetta[a], Mariella Dentini[a,*]

[a] Department of Chemistry, "Sapienza" University of Rome, P.le A.Moro 5, 00185 Rome, Italy
[b] Institute of Chemical Methodologies, CNR, Research Area of Rome, 00016 Monterotondo Staz., Rome, Italy
[c] Department of S.T.A.A.M., University of Molise, Via De Sanctis, 86100 Campobasso, Italy
[d] Department BAS, CR ENEA Trisaia, ss 106 jonica Km 419.5, 75026 Rotondella, Mt, Italy

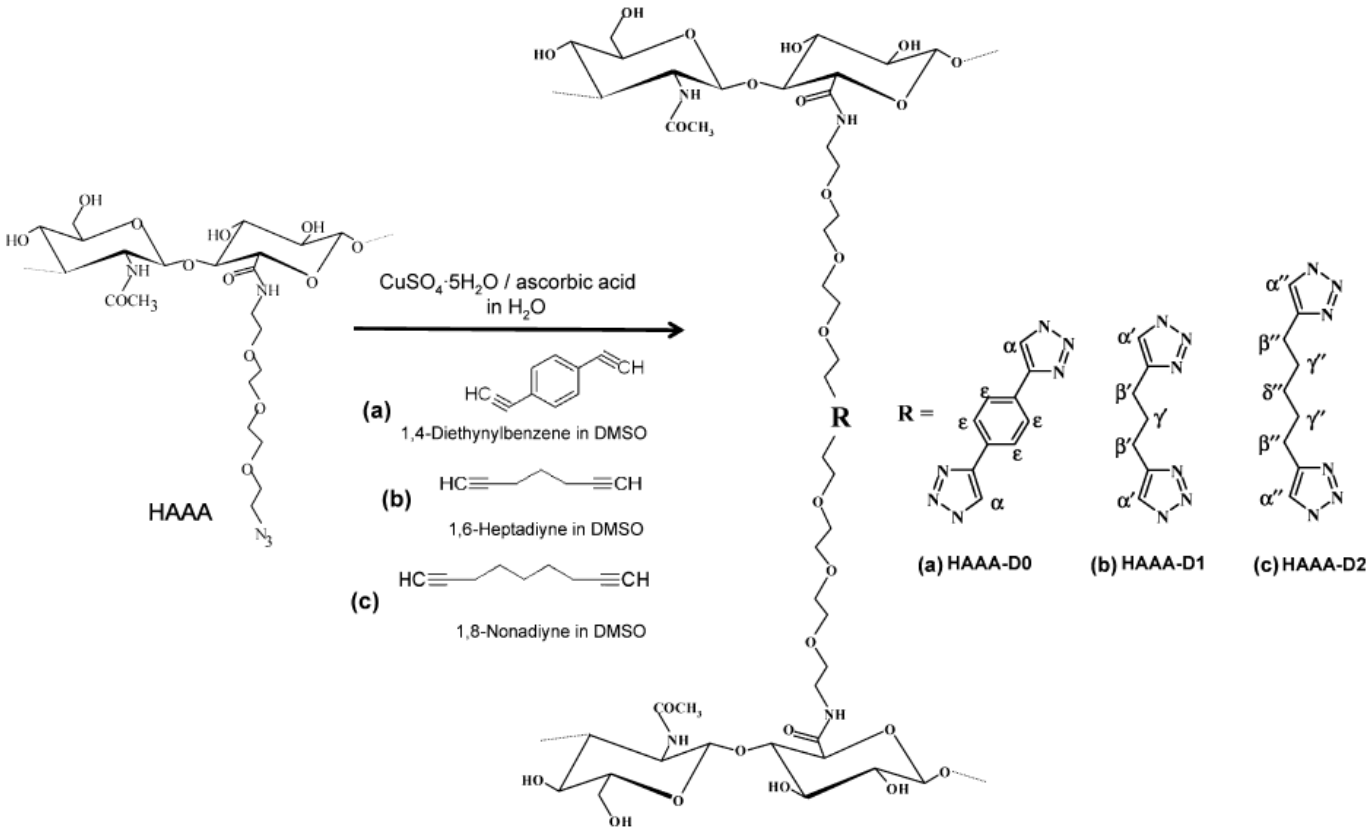

Scheme 1. Schematic representation of the HAAA-D0 (a), HAAA-D1 (b) and HAAA-D2 (c) click-gels formation.

Click gel

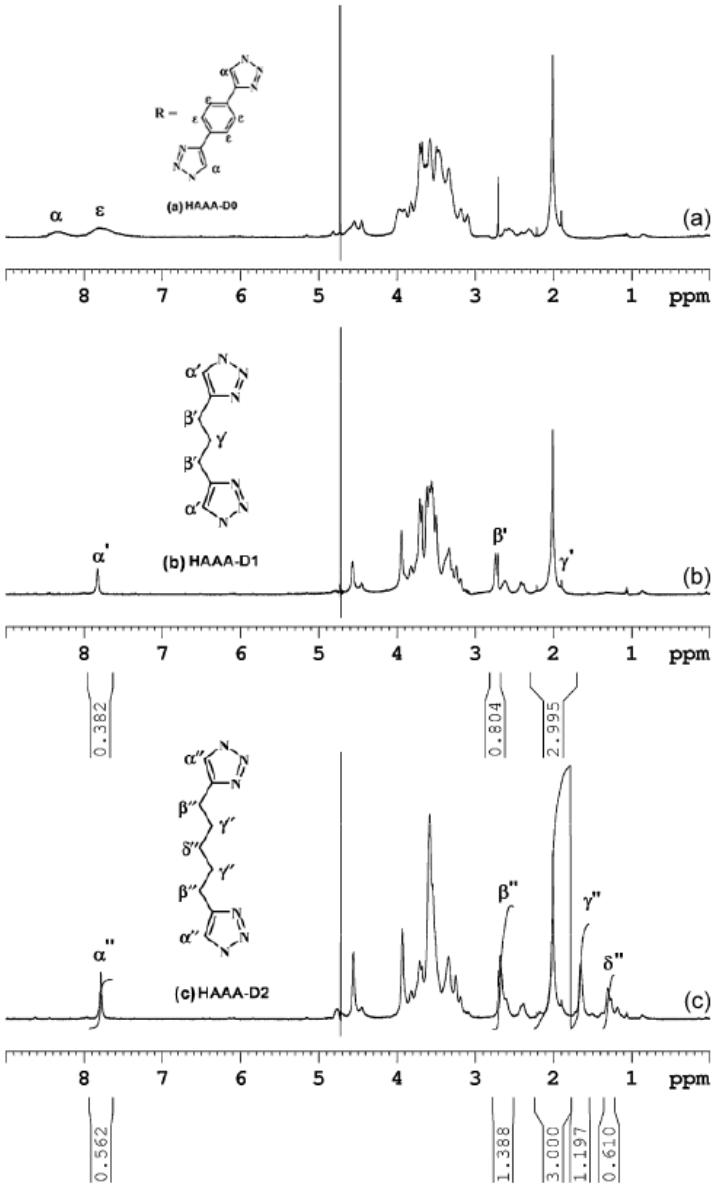

Fig. 2. 600.13 MHz ^{1}H HR-MAS spectra of HAAA-D0 (a), HAAA-D1 (b) and HAAA-D2 (c) click-gels hydrated with phosphate-buffered D_2O solution (100 mM, pD = 7) at $T = 27\,^{\circ}C$. The labels are used in accordance to Scheme 1a–c.

$$CD_b = \frac{\left(I(\alpha'/2\right)}{\left[\left(I(A) - I(\gamma')\right)/3\right]} \times 100 = 22\%$$

$$CD_c = \frac{\left(I(\alpha''/2\right)}{\left[(I(A))/3\right]} \times 100 = 28\%$$

Pullulan-NIPAAM gels.

NMR STUDY OF THERMAL TRANSITION OF N-ISOPROPYLACRYLAMIDE/METHACRYLATED PULLULAN HYDROGELS.

R.Lamanna[a], A.P. Sobolev[b], G. Masci[c], D.Bontempo[c], V. Crescenzi[c], and A.L. Segre[b]

a) CR ENEA Trisaia SS106 Jonica 75026 Rotondella (Mt), Italy
b) Institute of Chemical Methodologies, CNR M.B. 10, 00016 Monterotondo Stazione (Rome) , Italy
c) Department of Chemistry University of Rome "La Sapienza" P.le A. Moro 5, 00185 Rome, Italy

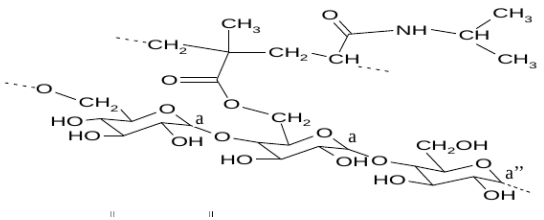

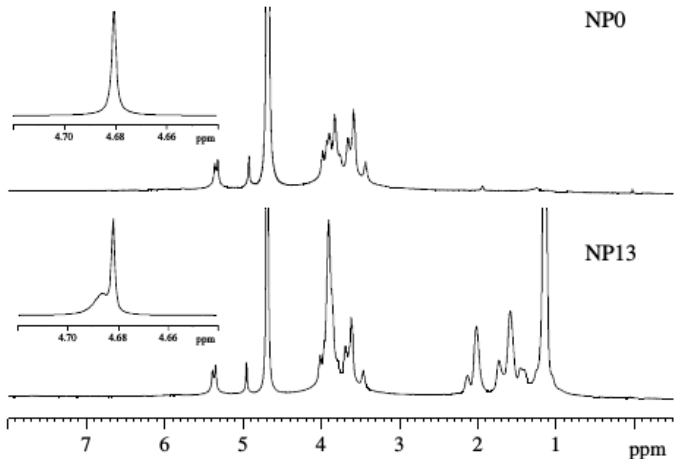

Figure 1. ^{1}H-HRMAS spectra of PULMA hydrogel with and without NIPAAM. The upper part of the spectrum represent the pure PULMA gel (NP0) whereas the lower part shows the PULMA-NIPAAM sample with 13 molecule of NIPAAM per methacrylate group (NP13). The insets show the corresponding water signals.

Thermal transition of Pullulan-NIPAAM gels.

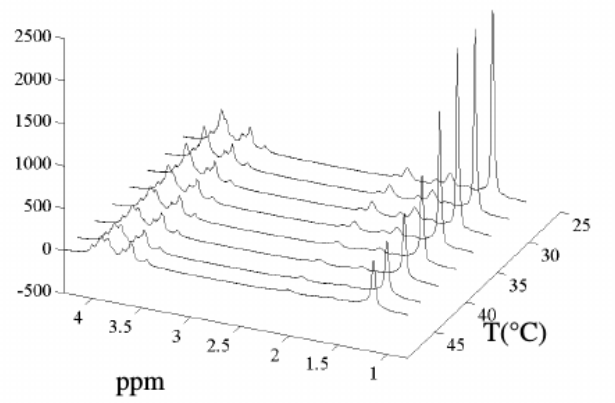

Figure 2. Stack plot of the NIPAAM and polysaccharide resonances as a function of temperature for the NP6 gel.

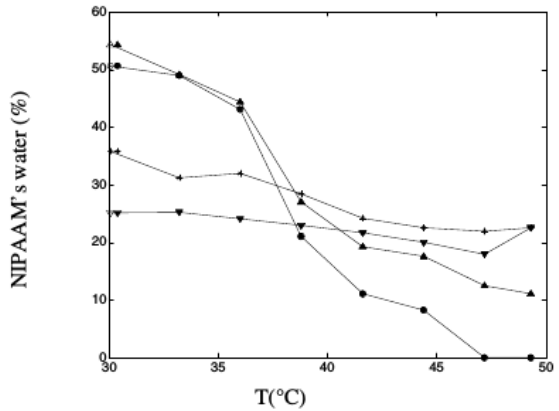

Figure 4. Bound water content as a function of temperature for gel with different amount of NIPAAM (NP3 down triangles, NP6 stars, NP10 up triangles, NP13 circles).

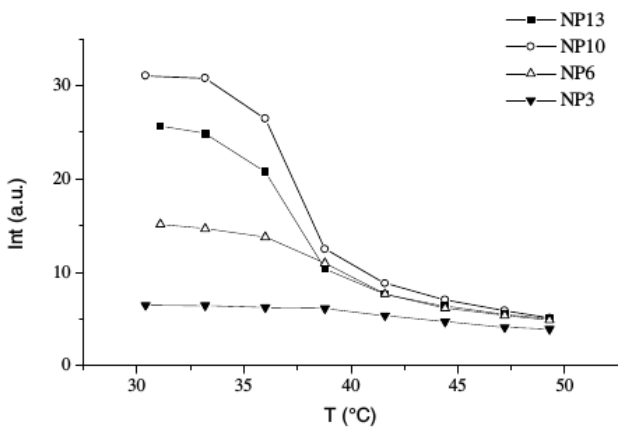

Figure 3. Intensity of methyl resonance of NIPAAM polymer as a function of temperature and for four hydrogel at different NIPAAM concentration.

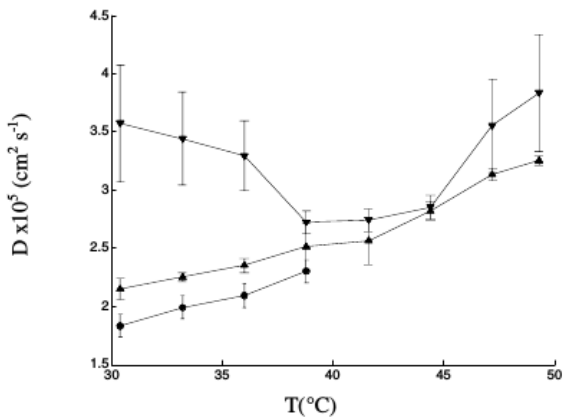

Figure 5. Self-diffusion coefficient of HOD as a function of the temperature for the NP13 gel. Up triangles represent the pure HOD self diffusion coefficients. Down triangles represent the diffusion coefficients of the high field water signal. The self diffusion coefficients of the bound water component are represented by filled circles.

Acta Biomaterialia 6 (2010) 3657–3664

Contents lists available at ScienceDirect

Acta Biomaterialia

journal homepage: www.elsevier.com/locate/actabiomat

Novel thermosensitive calcium alginate microspheres: Physico-chemical characterization and delivery properties

Letizia Oddo [a], Giancarlo Masci [b], Chiara Di Meo [a], Donatella Capitani [c], Luisa Mannina [c,d], Raffaele Lamanna [e], Serena De Santis [b], Franco Alhaique [a], Tommasina Coviello [a], Pietro Matricardi [a,*]

[a] Department of Drug Chemistry and Technologies, 'Sapienza' University of Rome, Place le A. Moro 5, 00185 Rome, Italy
[b] Department of Chemistry, 'Sapienza' University of Rome, Place le A. Moro 5, 00185 Rome, Italy
[c] Institute of Chemical Methodologies, CNR, Research Area of Rome, Via Salaria km 29,300, 00016 Monterotondo Stazione, Rome, Italy
[d] Department of S.T.A.A.M., University of Molise, Via De Sanctis, 86100 Campobasso, Italy
[e] Department BAS, CR ENEA Trisaia, ss 106 Jonica km 419.5, 75026 Rotondella, Mt, Italy

Thermosensitive Alg-Ca microspheres

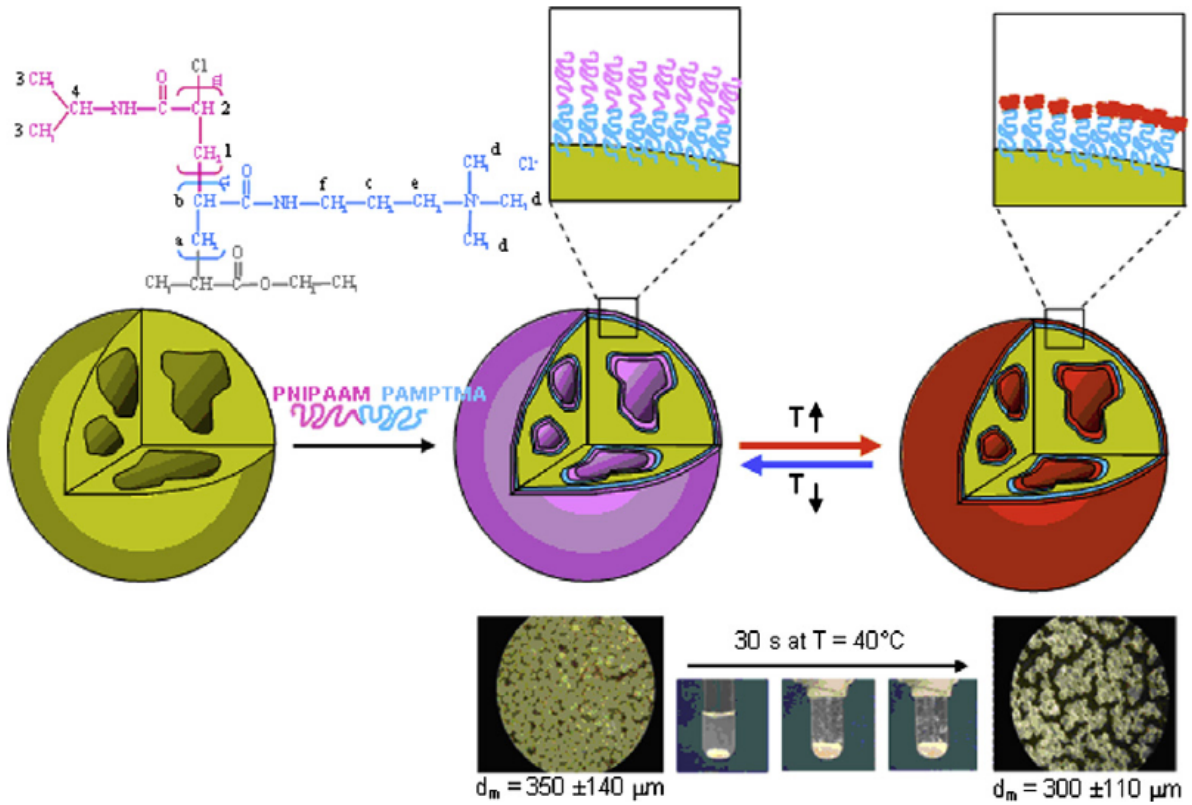

Fig. 1. Schematic representation of the CaAlg microsphere modification procedure and of the hydrophilic–hydrophobic thermal transition of the poly-NIPAAM moieties of the poly(AMPTMA-*b*-NIPAAM) anchored to the microspheres. The letters in the chemical structure refer to the NMR analysis. The pictures (below) show the evolution of a colloidal suspension of modified CaAlg microspheres [200 mg CaAlg, 0.5% (w/v) poly(AMPTMA-b-NIPAAM)] to a macroscopic aggregate. The mean diameter of the single microparticles (d_m) is also reported.

Thermosensitive Alg-Ca microspheres

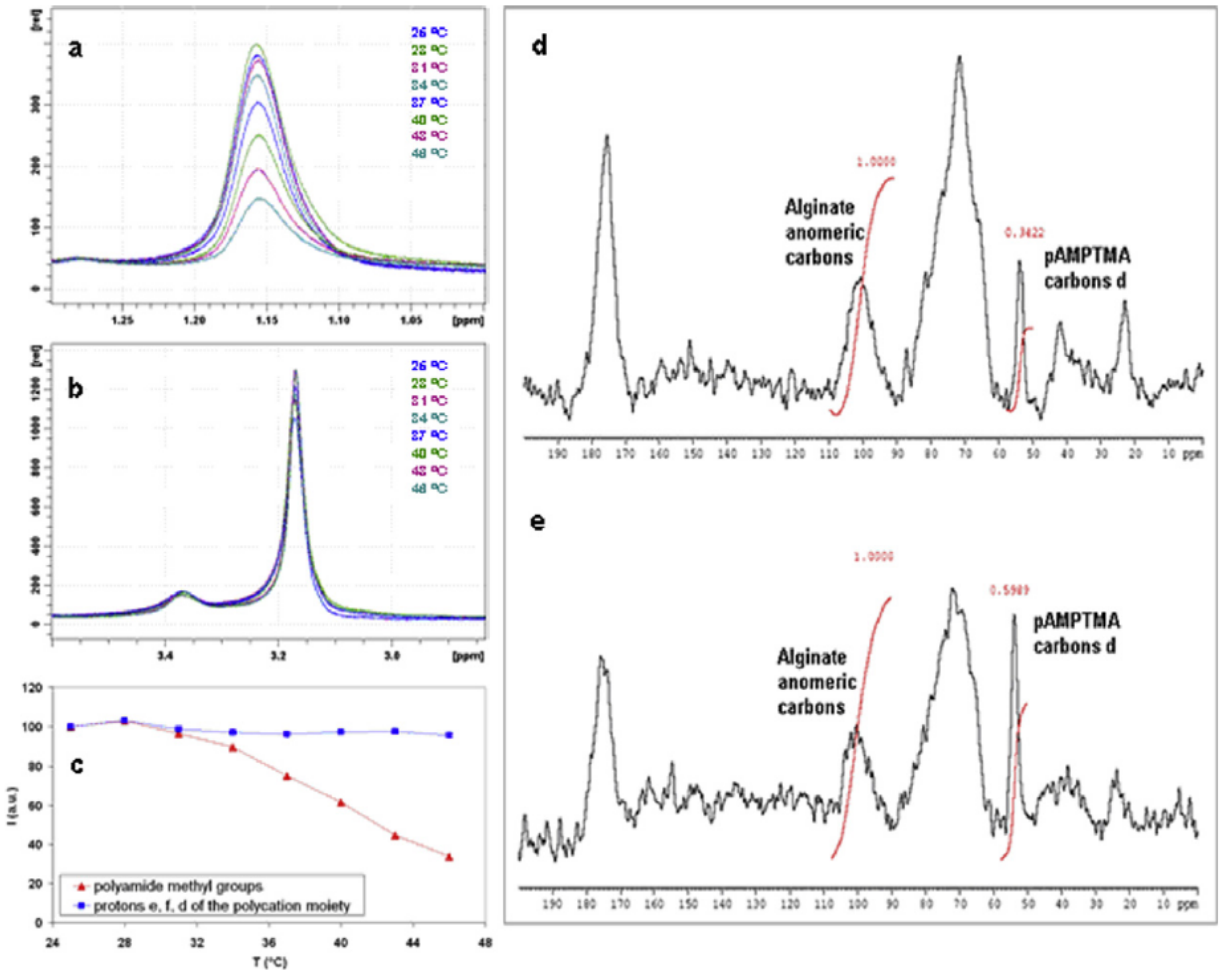

Fig. 2. 600.13 MHz ^{1}H HR-MAS spectra of poly(AMPTMA-*b*-NIPAAM)-modified CaAlg microspheres. (a) Resonances of the methyl groups of poly-NIPAAM at 1.1 ppm at different temperatures; (b) resonances of the poly(AMPTMA) moiety in the 2.9–3.7 ppm range at different temperatures; (c) integrals of the signals recorded in (a) and (b) reported as a function of temperature. 50.13 MHz ^{13}C MAS NMR spectra of poly(AMPTMA-*b*-NIPAAM)-modified CaAlg microspheres obtained with 0.5% (w/v) (d) and 1.5% (w/v) (e) aqueous solutions of poly(AMPTMA-*b*-NIPAAM). The integrals for estimation of the ratio between AMPTMA repeating units and uronic residues of alginate are also reported.

Diffusione in sistemi eterogenei

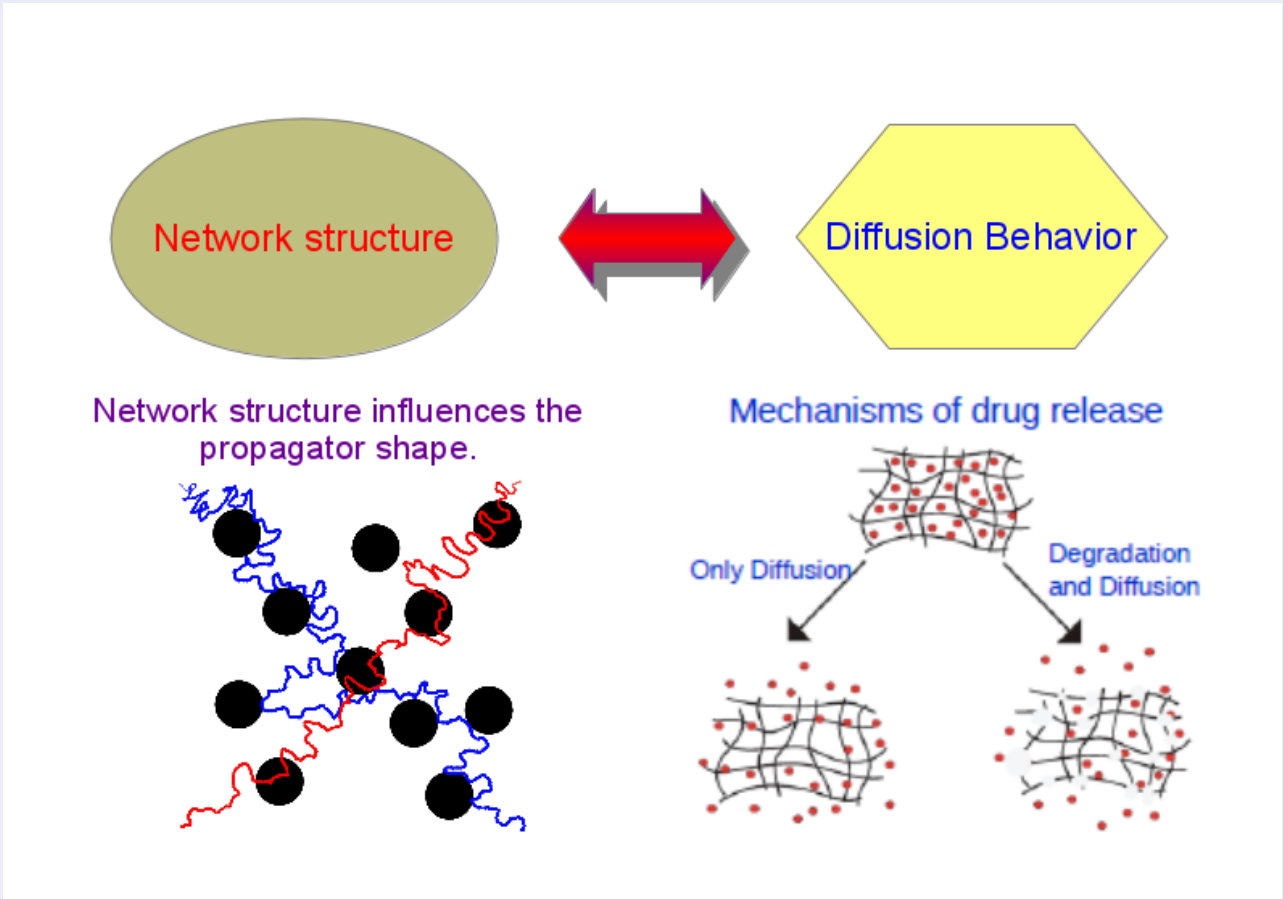

Diffusion
NMR measurements

- $E(q,t_d) = \int \overline{P}(\mathbf{z},t_d) e^{(i\mathbf{q}\cdot\mathbf{z})} d\mathbf{z}$
  $\mathbf{q} = \gamma\delta\mathbf{g}$
- $E(q,t_d) = exp(-q^2\overline{z^2}(t_d))$
- $\overline{z^2}(t_d) = \int z^2\ \overline{P}(z,t_d)dz$

$$\overline{z^2}(t_d) = Kt_d^{\gamma}$$

$\gamma < 1$	Subdiffusion
$\gamma = 1$	Gaussian
$1 < \gamma < 2$	Superdiffusion

NMR Echo Decays

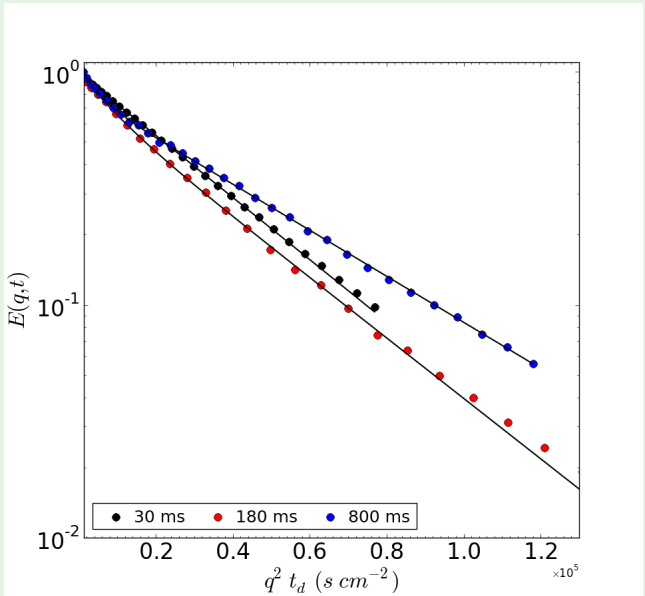

Fourier Transform of ED

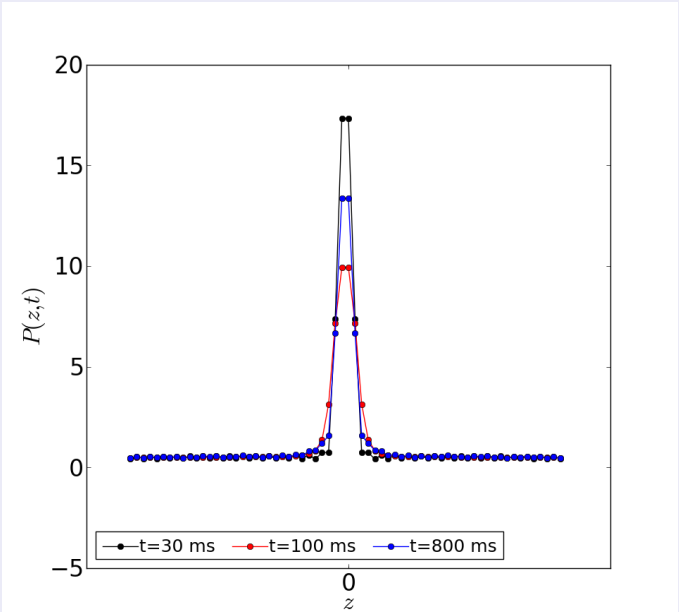

Gaussian vs. Anomalous

$$E(q, t_d) = exp(-q^2 \overline{z^2}(t_d))$$

$$\overline{z^2}(t_d) = \int z^2 \, \overline{P}(z, t_d) dz$$

Gaussian $\overline{z^2}(t_d) = 2Dt_d$

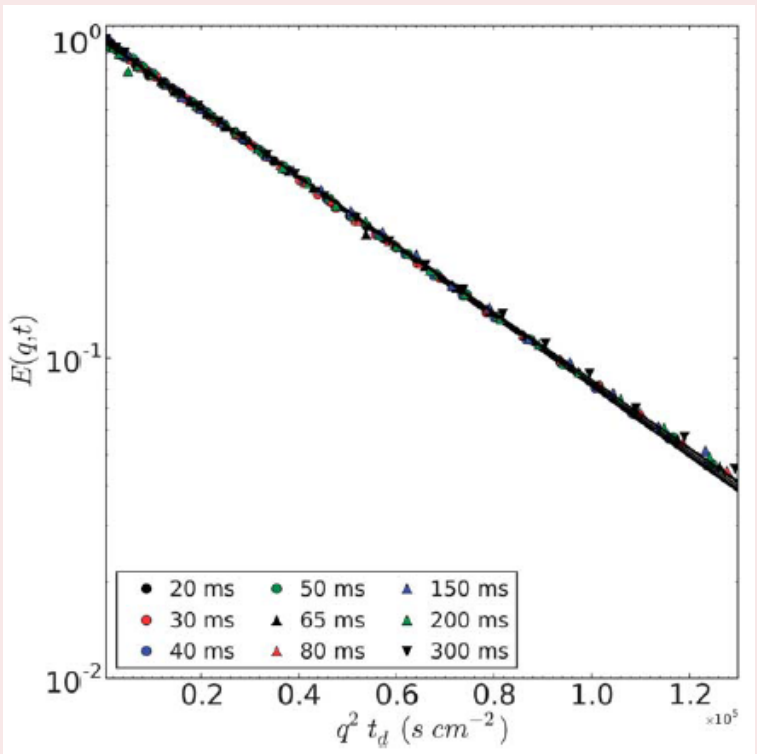

Enhanced Diffusion

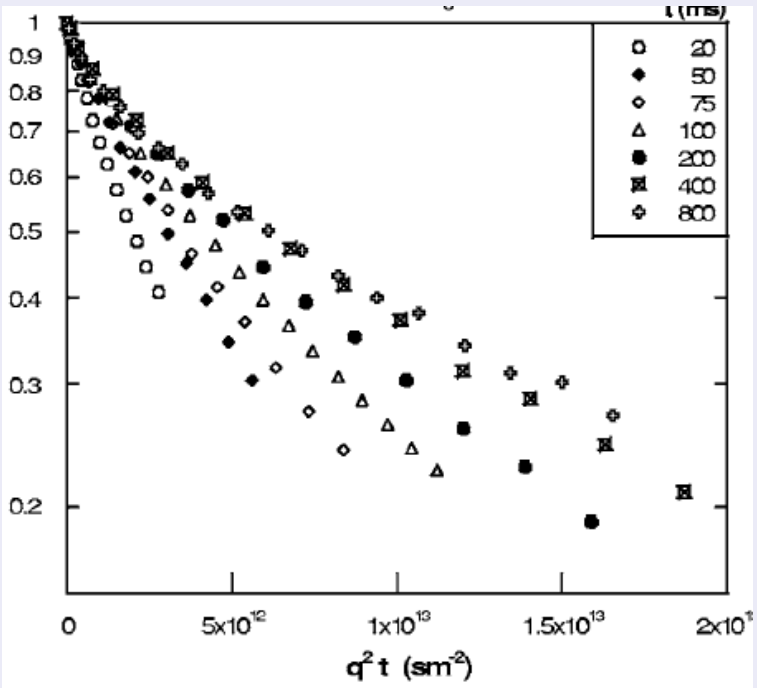

Scleroglucan/Borax Gels

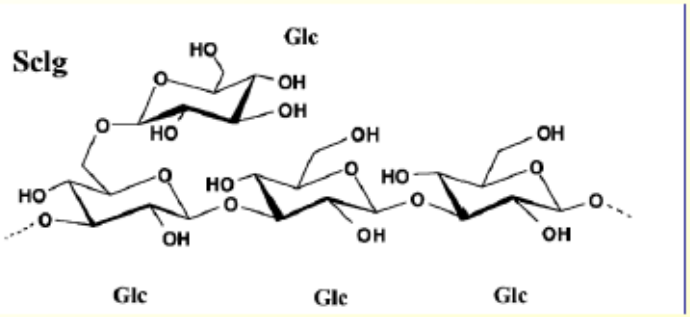

+ $Na_2B_4O_7$ = in H_2O

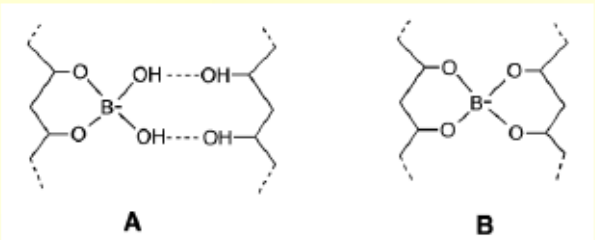

chemical/physical (A) and chemical/chemical (B) linkages.

24 h

Hydrogel

Freeze-drying

Compression

(5 kN for 30 s)

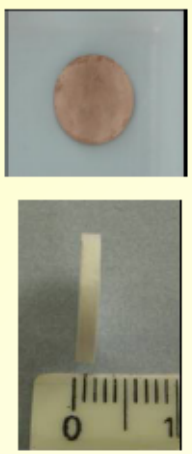

Sclg/borax tablet

Swelling

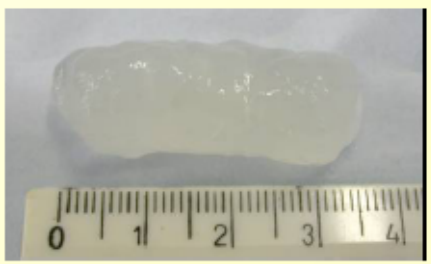

Scleroglucan: one of the most rigid polymers in nature

Persistence lenght: 200 nm

Solid state and aqueous solution (pH < 14):
Triple helix ⟶ TRIPLEX

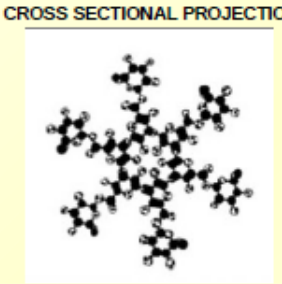

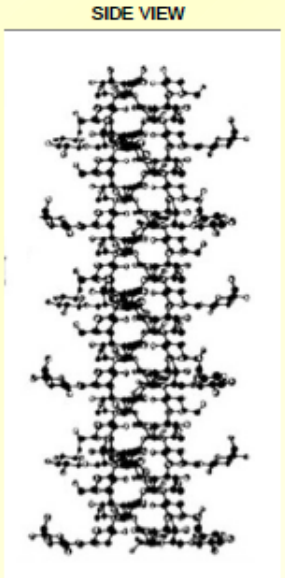

Maeda *et al.*, Int. J. Biol. Macromol, 28, 2001

MD studies on Sclg-borax hydrogels:

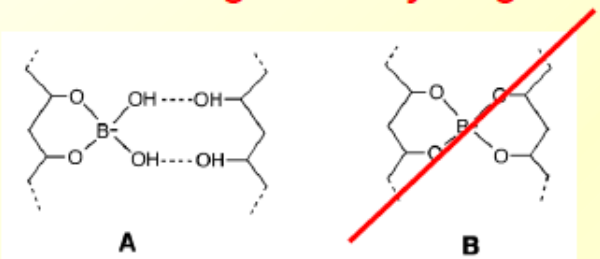

BORAX ⟹ Links the Sclg triplexes stabilizing inter-triplex interactions.
Leads to the formation of ordered domains

Parallel stiff triplexes
⇩
Formation of nanochannel-like structures

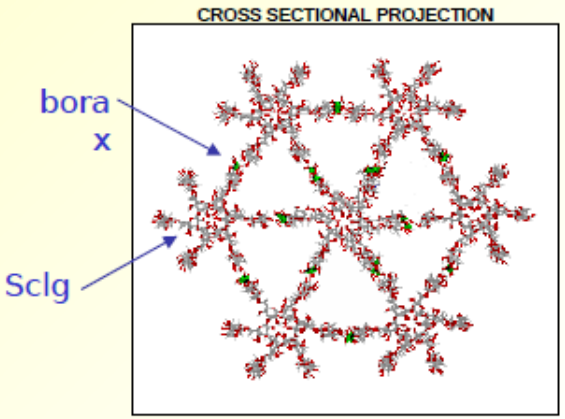

Bocchinfuso *et al.*, J. Phys. Chem. B, Vol. 112, No. 20, 2008

Water diffusion in sgleroglucan gels

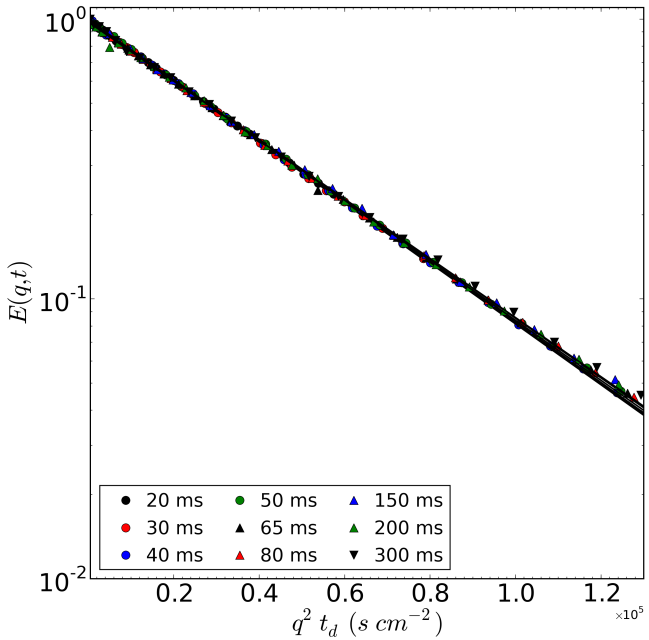

NMR decay of water in the Sclg sample *vs.* $q^2 t_d$.

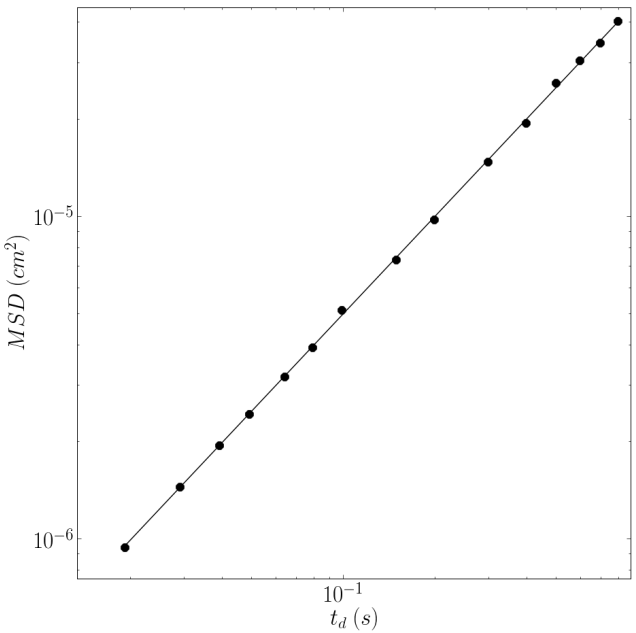

MSD of water in the Sclg sample

$D = 2.51 \pm 0.03 \times 10^{-5} cm^2 s^{-1}$
$\gamma = 1.00 \pm 0.01.$

"Anisotropic enhanced water diffusion in sclerogluca gel tablets" Chiara Di Meo, Tommasina Coviello, Pietro Matricardi, Franco Alhaique, Donatella Capitani and Raffaele Lamanna* **Soft Matter**, (2011),7, 6068-6075

Scleroglucan Borax

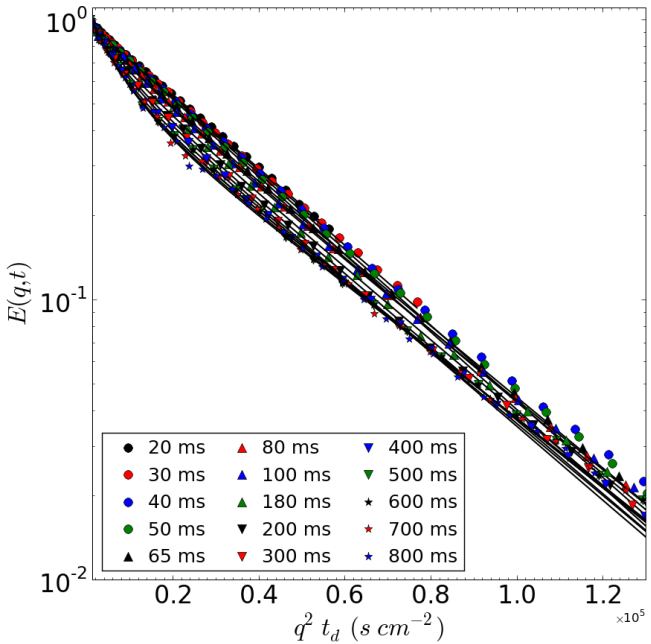

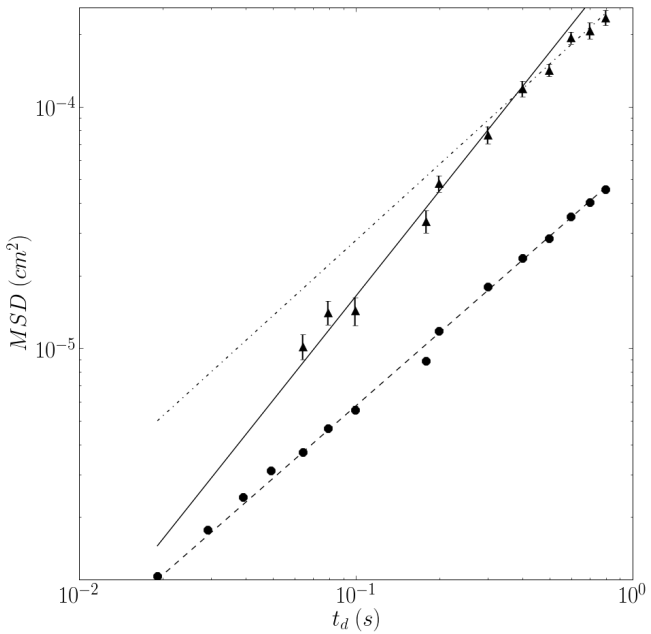

Slow component

$D = 2.90 \pm 0.04 \times 10^{-5} cm^2\ s^{-1}$

$\gamma = 1.00 \pm 0.02$

Fast component

$K = 46 \pm 14 \times 10^{-5} cm^2\ s^{-1.4}$

$\gamma = 1.4 \pm 0.2$

$D = 15 \pm 1 \times 10^{-5} cm^2\ s^{-1}$

$\gamma = 1.0 \pm 0.1$

Scleroglucan Borax Compressed

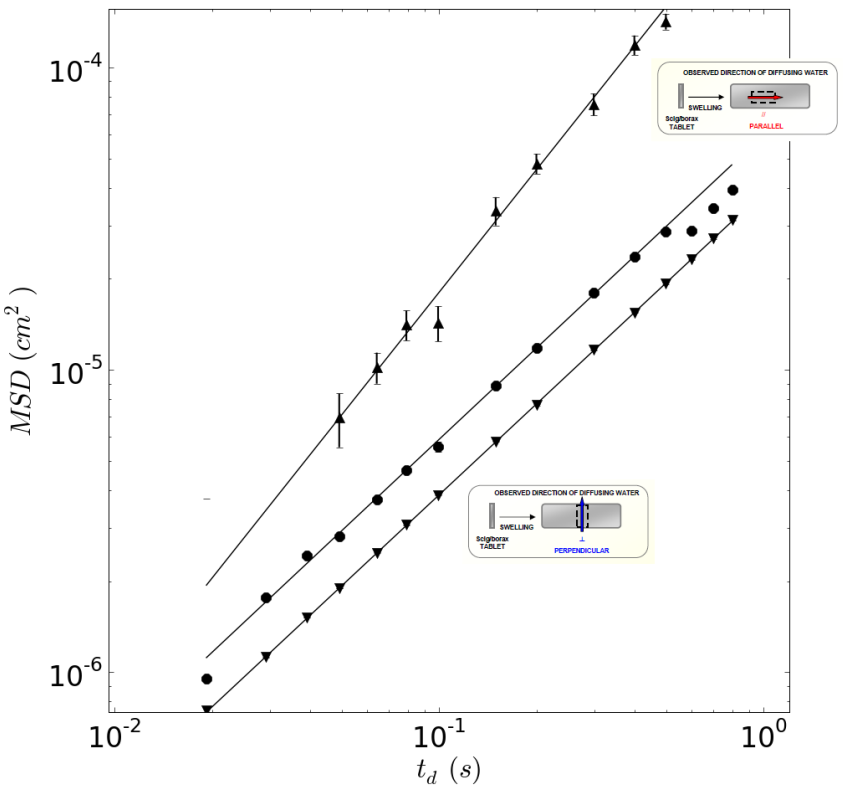

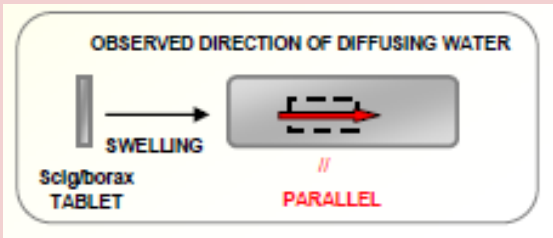

- $K = 40 \pm 2 \times 10^{-5} cm^2\ s^{-1.35}$
  $\gamma = 1.35 \pm 0.04$
- $D = 3.00 \pm 0.03 \times 10^{-5} cm^2\ s^{-1}$

  $\gamma = 1.006 \pm 0.008$

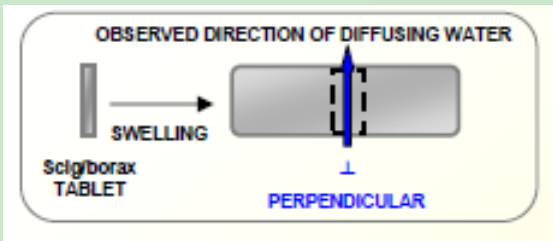

$D = 1.940 \pm 0.003 \times 10^{-5} cm^2 s^{-1}$

$\gamma = 1.002 \pm 0.002$

The fraction of SMD molecules.

The $t^{3/2}$ dependence of MSD is observed mainly due to the behaviour of a small fraction of diffusing molecules performing large bulk excursions. This fraction of diffusing molecules is time dependent and is given by:

$$h = \sqrt{\frac{t}{t_h}}$$

where t_h is the retention time.

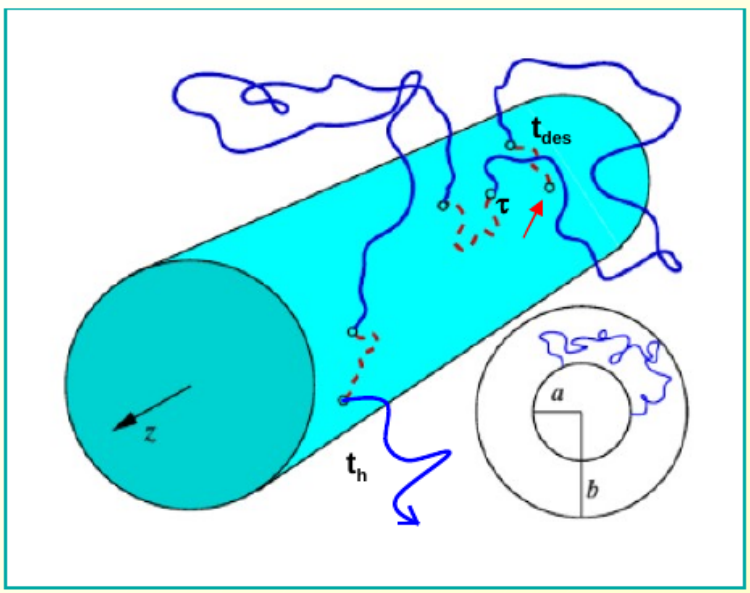

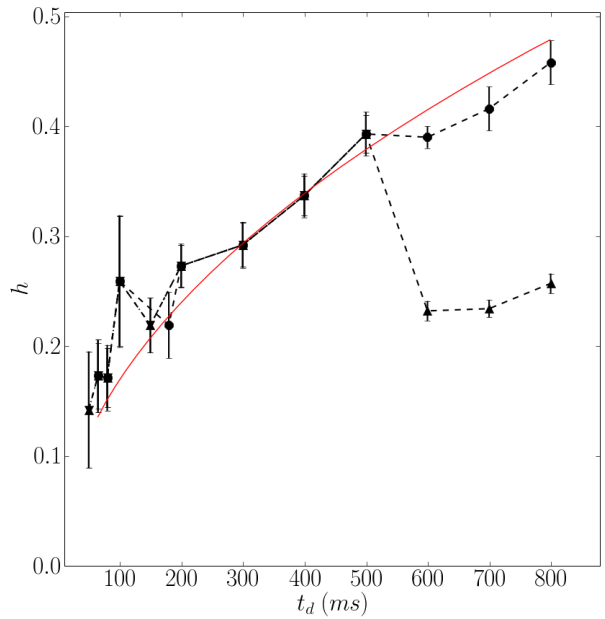

Relative intensity of water diffusion fraction *vs.* $q^2 t_d$. (●): Sclg/borax R=0.5 uncompressed, (▲): components along the compression direction (||) of Sclg/borax tablet R=0.5,(▼) components along the compression direction (||) of Sclg/borax tablet R=1.0.

IPN

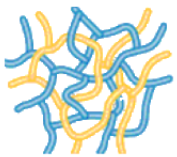

IPN

Two independently crosslinked polymeric networks (A-A / B-B) form a completely entangled system

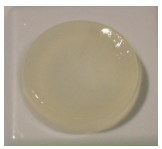

IPN AlgCa/HAMAg

calcium alginate (AlgCa)

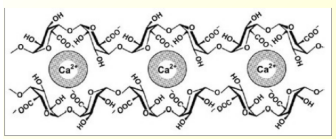

methacrylated hyaluronic acid (HAMA)

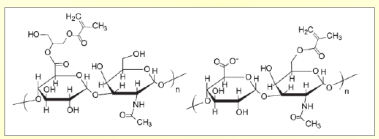

Water Signals

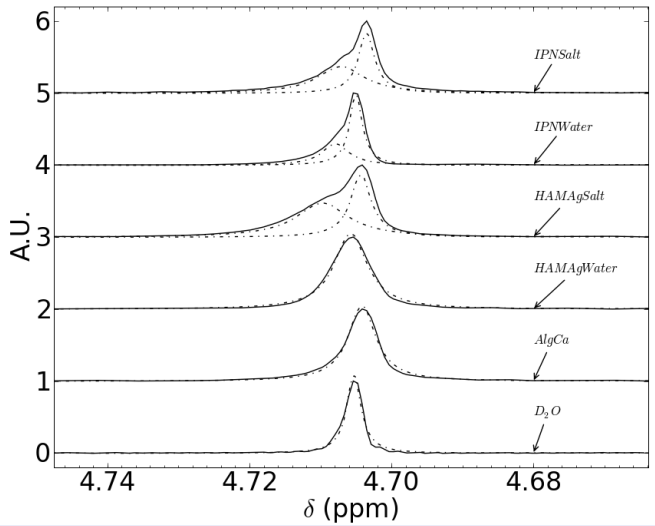

Sample	Chemical shift (ppm)	Relative amount (%)	Linwidth (Hz)
$H_2O - D_2O 95\%$	×	100	1.53
$AlgCa$	4.7042	100	2.27
$HAMAg - H_2O\ \alpha$	4.7059	100	3.44
$HAMAg - NaCl\ \alpha$	4.7039	42.1	2.16
$HAMAg - NaCl\ \beta$	4.7094	57.9	5.48
$IPN\ \alpha$	4.7045	61.3	2.73
$IPN\ \beta$	4.7076	38.7	5.71
$IPN - NaCl\ \alpha$	4.7030	44.2	1.71
$IPN - NaCl\ \beta$	4.7076	55.8	4.88

Table 1: Relative amount and line-width of the water fitting components for all the samples.

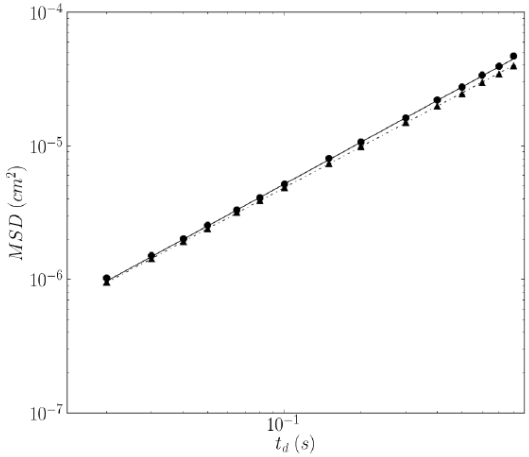

Figure 2: HAMAg prepared in distilled water (dots) and AlgCa (triangles). MSD of water vs. the diffusion time. Solid line fit of HAMAg prepared in distilled water with $D = 2.490 \pm 0.007 \times 10^{-5} cm^2 s^{-1}$ and $\gamma = 0.996 \pm 0.004$. Dashed line fit of AlgCa data with $D = 2.88 \pm 0.02 \times 10 - 5cm2s - 1$ and $\gamma = 1.04 \pm 0.01$

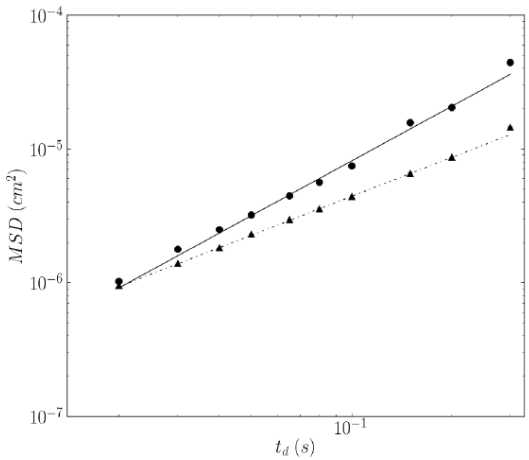

Figure 4: HAMAg prepared in NaCl 0.9% (w/v): MSD of water vs. the diffusion time. Dots, water resonance at 4.704 ppm. Dashed line fit with $K = 10.5 \pm 0.8 \times 10 - 5cm2s - 1.27$ and $\gamma = 1.27 \pm 0.03$. Triangles, water resonance at 4.709 ppm. Solid line fit with $K = 1.71 \pm 0.1 \times 10 - 5cm2s - 0.93and\gamma = 0.93 \pm 0.03$.

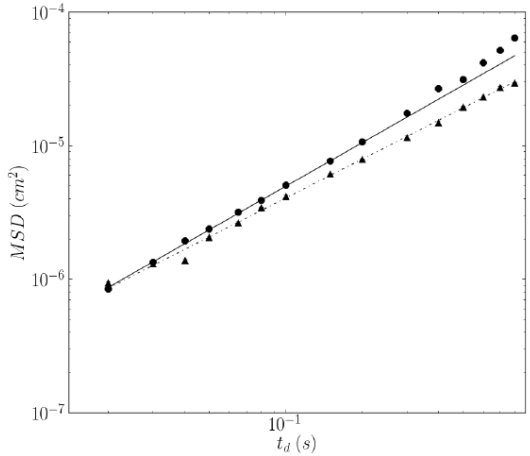

Figure 3: IPN prepared in water: MSD of water vs. the diffusion time. Dots, water resonance at 4.703 ppm. Dashed line fit with $K = 2.93 \pm 0.08 \times 10^{-5} cm^2 s^{-1.07} and \gamma = 1.07 \pm 0.04$. Triangles, water resonance at 4.708 ppm. Solid line fit with $D = 2.30 \pm 0.05 \times 10^{-5} cm^2 s^{-1} and \gamma = 1.02 \pm 0.03$.

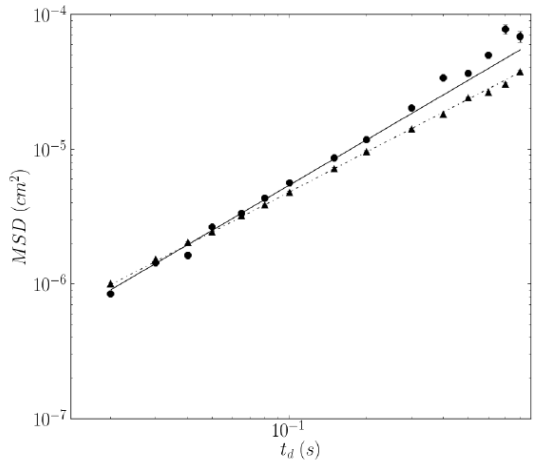

Figure 5: IPN prepared in NaCl 0.9%. (w/v): MSD of water vs. the diffusion time. Dots, water resonance at 4.703 ppm. Dashed line fit with $K = 5.6 \pm 0.4 \times 10 - 5cm2s - 1.28$ and $\gamma = 1.28 \pm 0.03$. Triangles, water resonance at 4.708 ppm. Solid line fit with $K = 2.06 \pm 0.03 \times 10 - 5cm2s - 0.92$ and $\gamma = 0.92 \pm 0.05$.

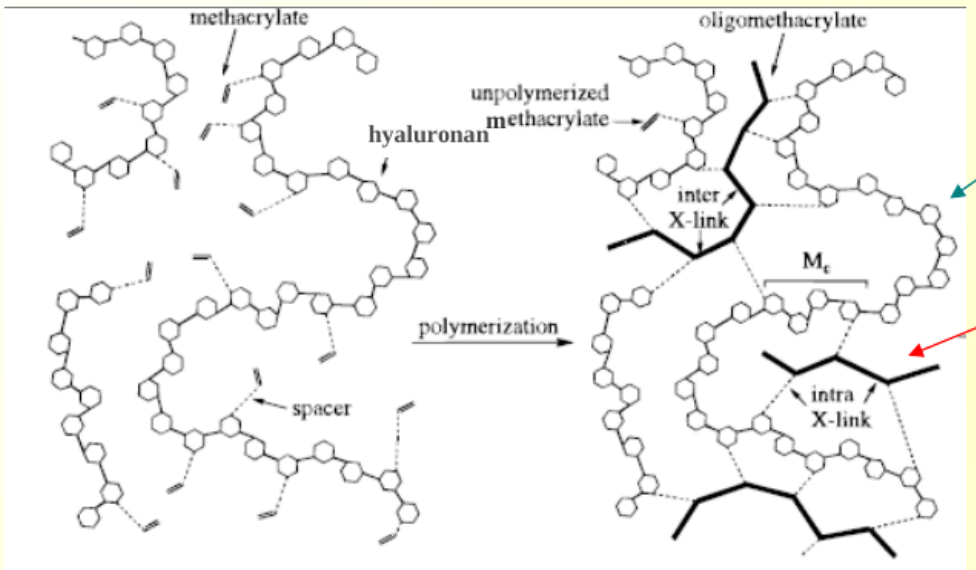

Hydrophilic domains

Hydrophobic domains

Polimeri

- Nei polimeri solo una piccola frazione di catene mobili é visibile in HRMAS
- Il segnale ridotto delle catene polimeriche favorisce la rivelazione dei contaminanti o delle sostanze attive inglobate.

Polimeri attivi

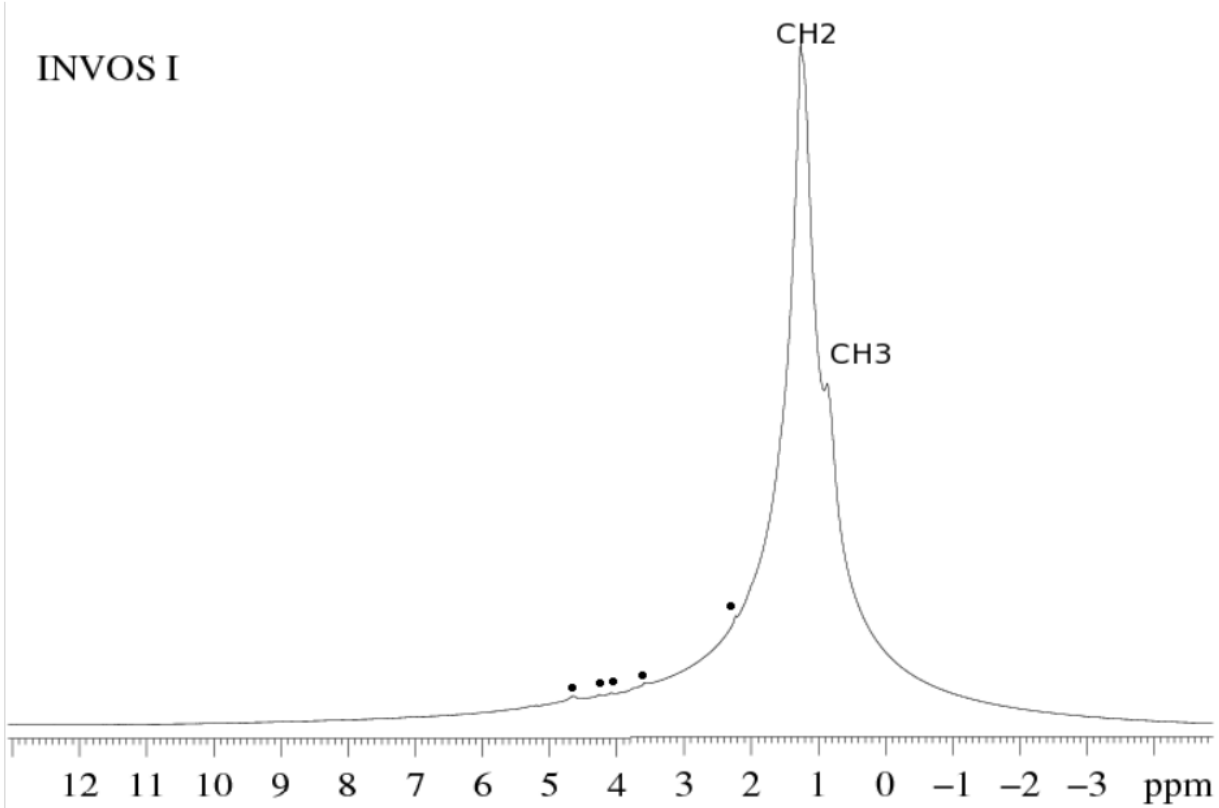

Figure 1: 1H HRMAS NMR spectrum of Invos1 LDPE polymer.

In the spectrum, the mobile chain of the polymer are clearly visible as a very broad line around 1.2 ppm. Despite the large linewidth it is possible to distinguish CH2 and CH3 groups of the polymer. At lower field small lines, marked with dots, represent the compounds of Nisaplin formulation added in the lacquer. Actually, Nisaplin is a commercial formulation containing 2.5 % of nisin, 77.5% of NACl, 12% of proteins, 6% of carbohydrates and 2% moisture.

Signal suppression & filtering

1H MAS

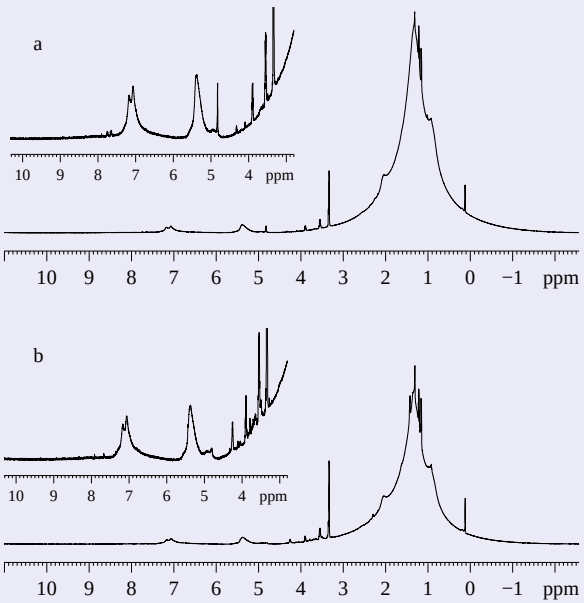

a) LDPE+PVC ; b) LDPE+PVC+Nisina

1H MAS T2 Filtered

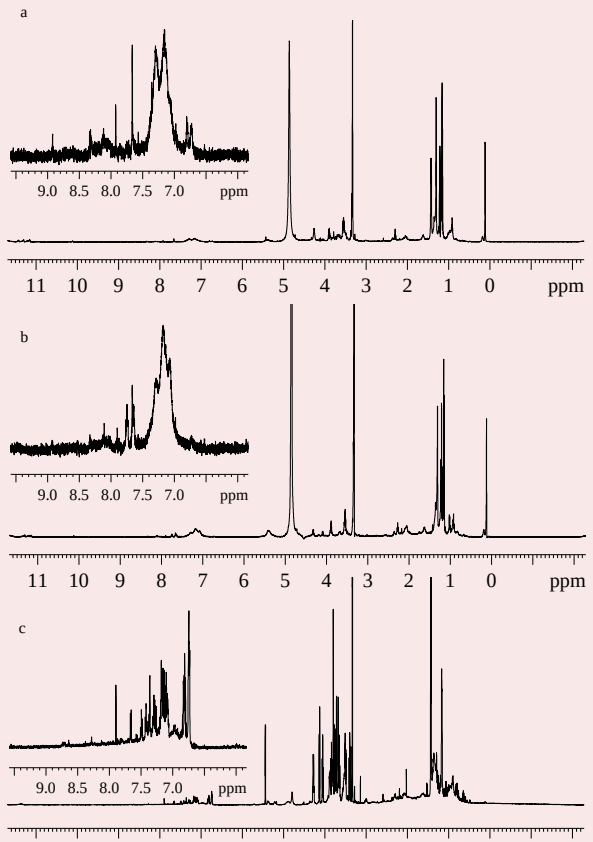

a) LDPE+PVC+Nisina ; b) LDPE+PVC; c) Nisina

Confronto fra polimeri

HDPE

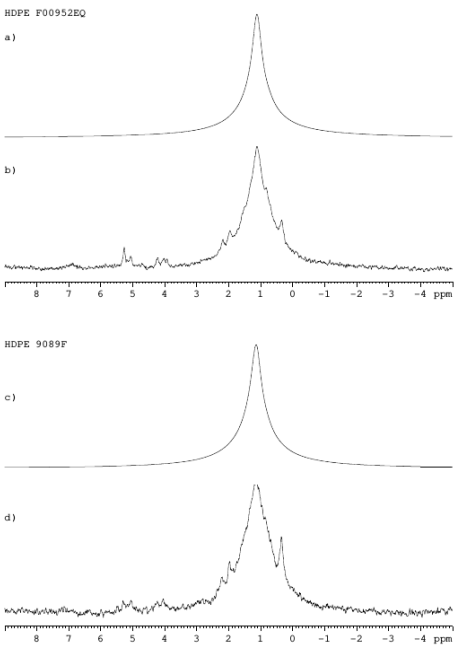

Figura 1: Spettri 1H HR-MAS NMR di campioni di polietilene ad alta densità (HDPE)

LDPE

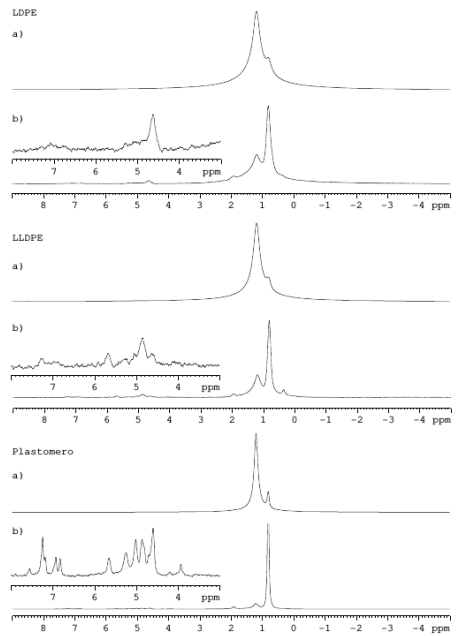

Figura 2: Spettri 1H HR-MAS NMR di campioni di polietilene bassa densità: 1.LDPE; 2. LLDPE; 3. Plastomero). Gli inserti mostrano espansioni dello spettro nelle regioni in cui emergono segnali di componenti minoritari.

O

Contaminazione esterna (olio d'oliva)

HDPE

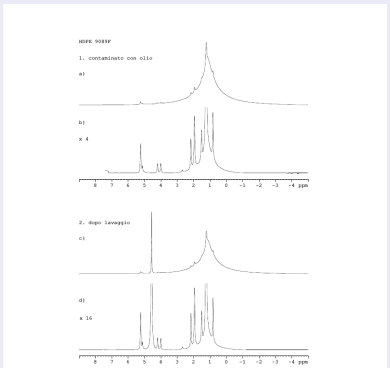

Figura 5: Spettri 1H HR-MAS NMR di HDPE 9089F: (a,b) contaminato con olio d'oliva; (c,d) dopo lavaggio.

LDPE

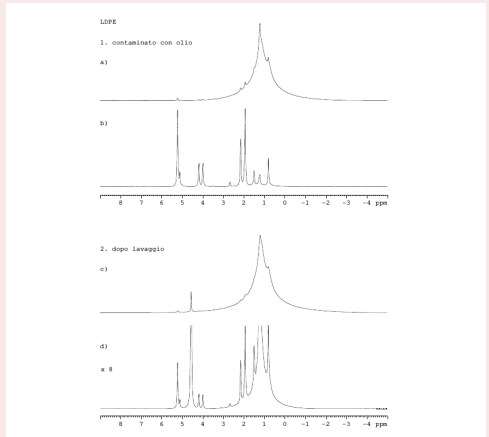

Figura 6: Spettri 1H HR-MAS NMR di LDPE: (a,b) contaminato con olio d'oliva; (c,d) dopo lavaggio.

LLDPE

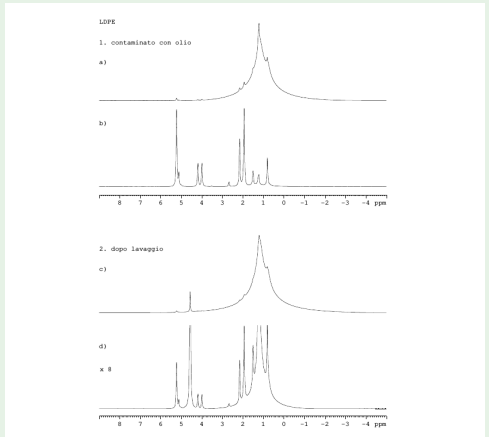

Figura 6: Spettri 1H HR-MAS NMR di LDPE: (a,b) contaminato con olio d'oliva; (c,d) dopo lavaggio.

Contaminazione esterna (passata di pomodoro)

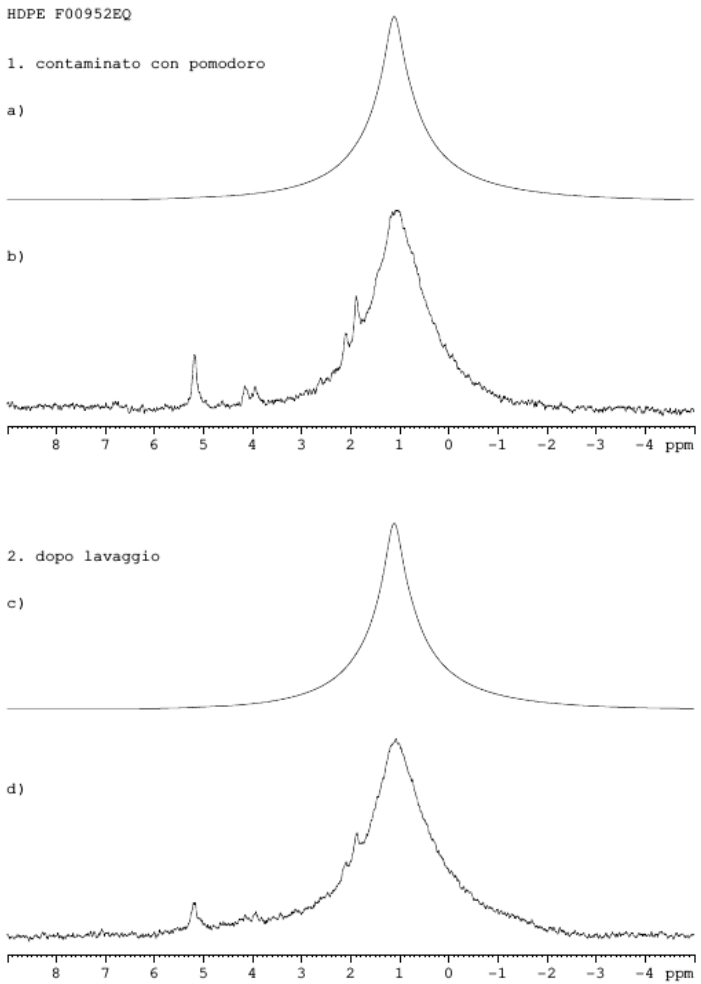

Figura 9: Spettri 1H HR-MAS NMR di HDPE F00952EQ: (a,b) contaminato co conserva di pomodoro; (c,d) dopo lavaggio.

Food contact

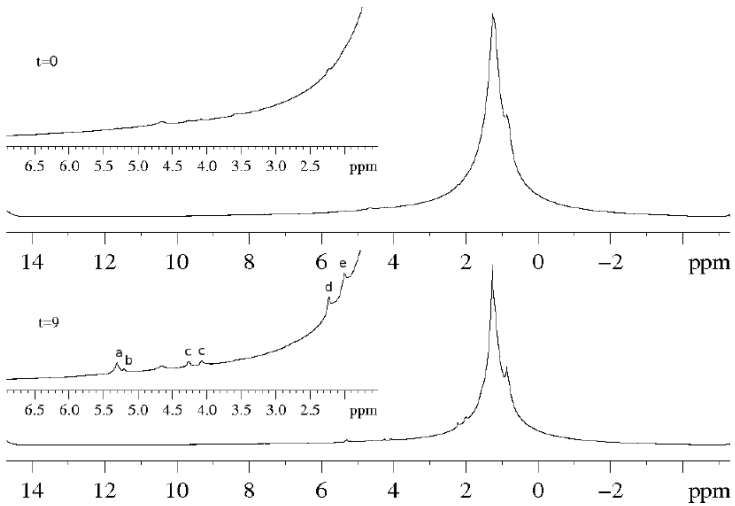

Figure 2: 1H HRMAS NMR spectrum of Invos 1 film before and after contact with cheese.

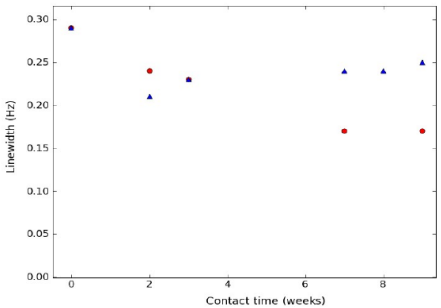

Figure 5: Linewidth of the sharp deconvolution Lorentzian vs packaging time: Invos1 film (red circles), Invos2 film (blue triangle)

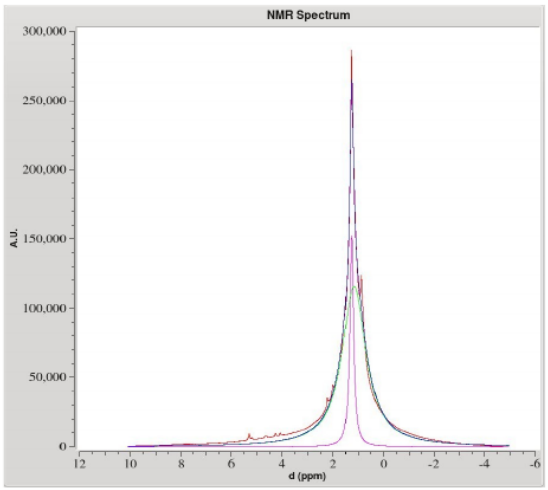

Figure 3: Spectrum deconvolution of Invos 1 film

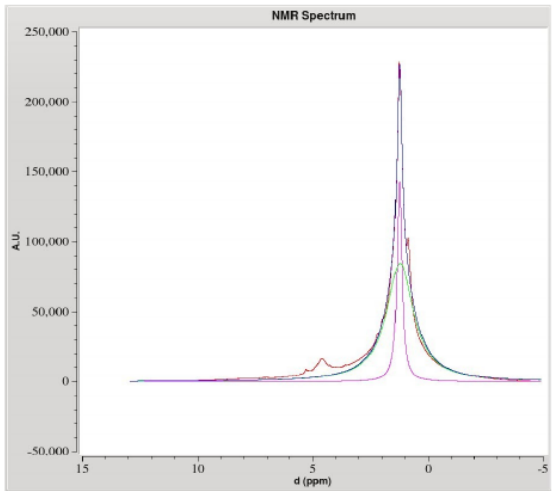

Figure 4: Spectrum deconvolution of Invos2 film

Film	Not used film	SILANO 1 week	SILANO 6 weeks	SILANO 10 weeks
INVOS I	1.6±0.8	3.3; 4.5	8.8; 12.2	12.3; 14.5
INVOS II	1.8±1.0	2.3; 4.7	3.9; 7.3	9.5; 14.1

Commercial film food contact

LDPE-without PVC

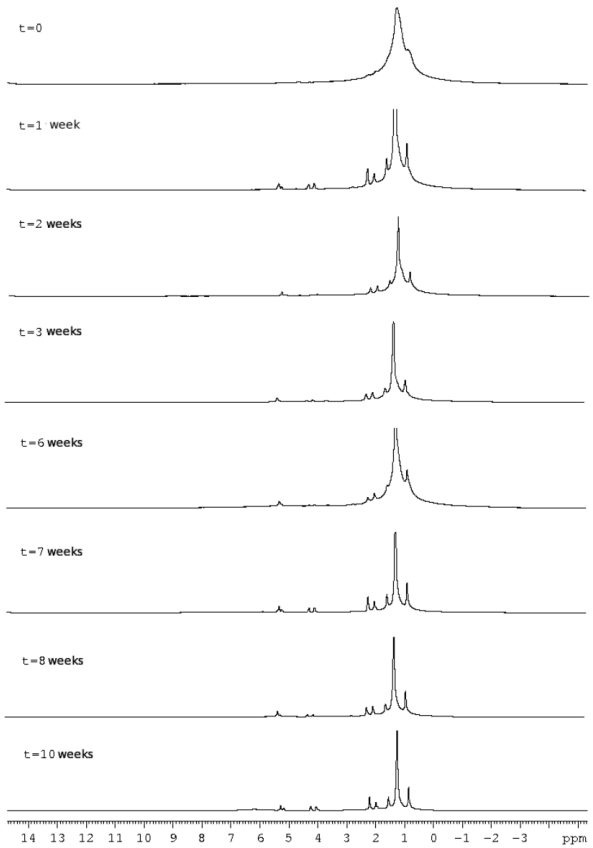

Figure 7: Spectra of GS-film for different time of exposition to cheese.

LDPE with PVC

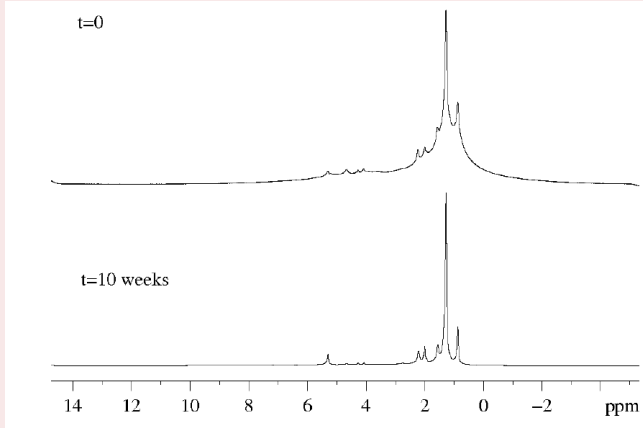

Figure 8: Spectra of GSPVC-film not suitable for cheese packaging at two exposition times.

Migration into food
Provolone cheese

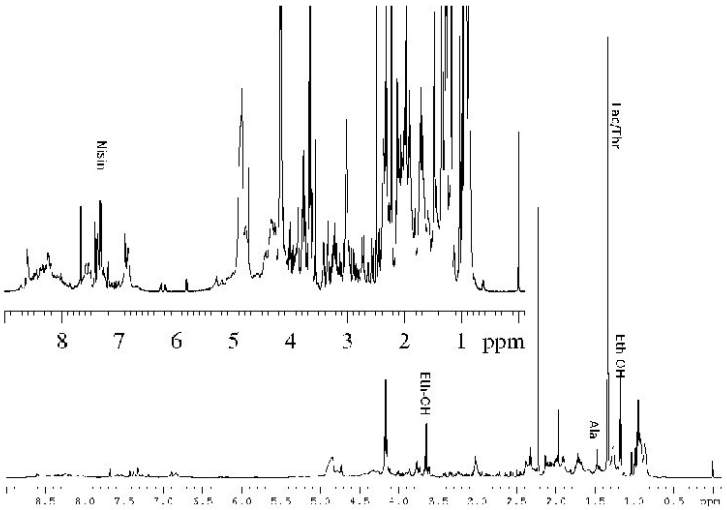

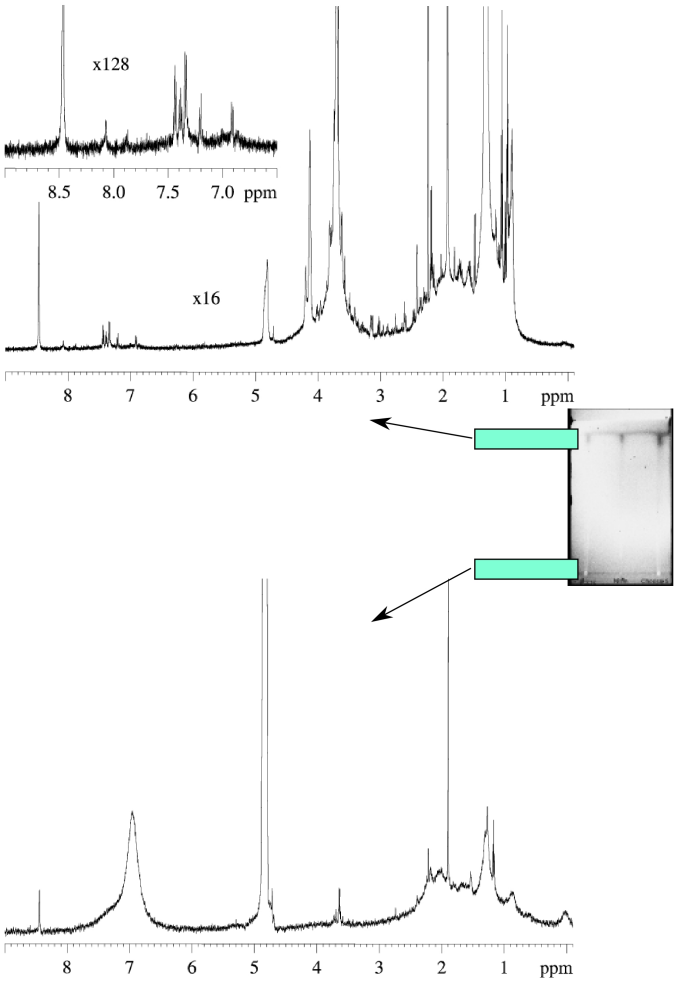

Migration into simulants

Test with fatty simulants.

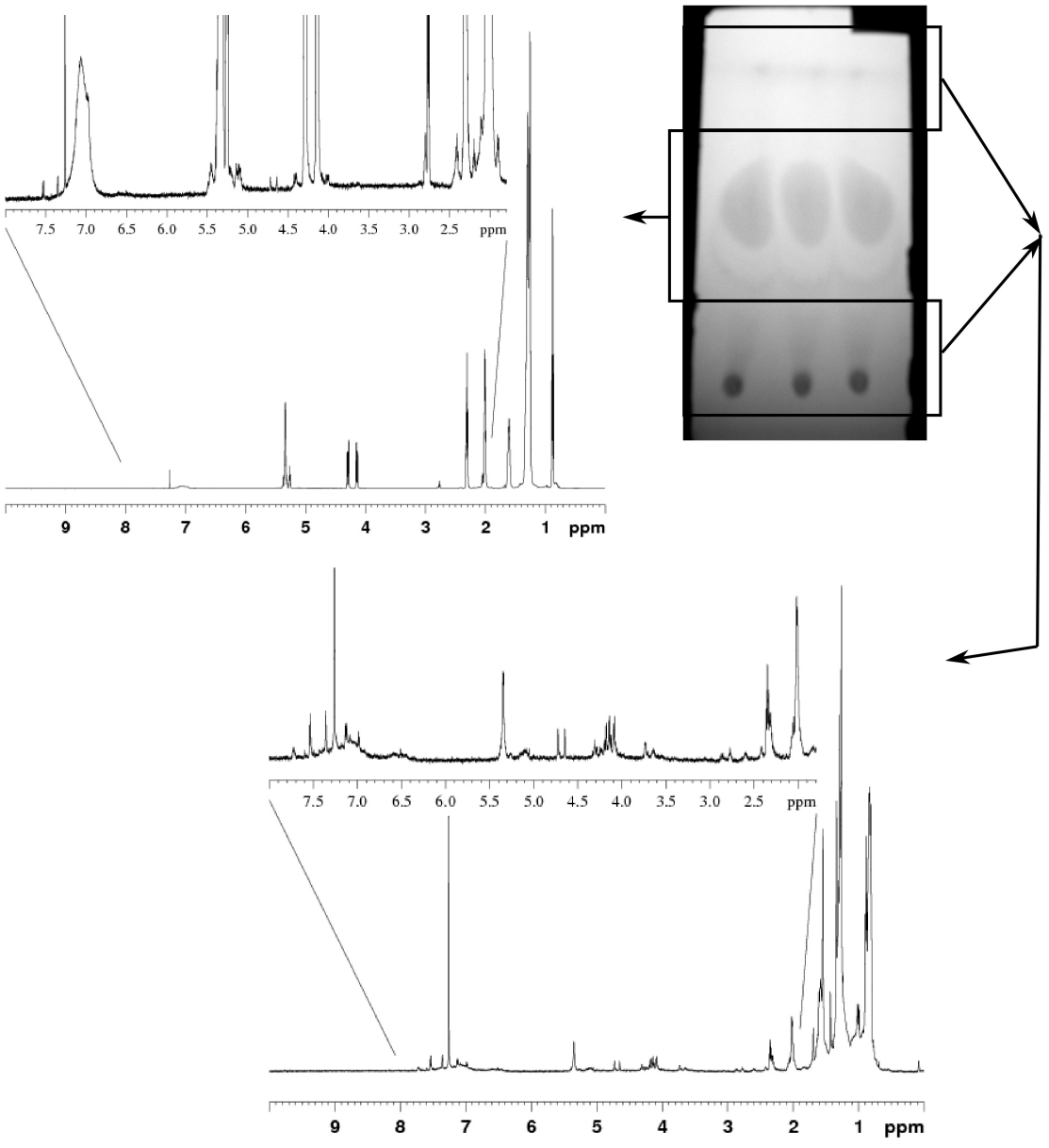

Chromatographic MAS NMR

Annual Reports on
NMR SPECTROSCOPY

VOLUME **73**

Edited by

GRAHAM A. WEBB
Royal Society of Chemistry
Burlington House
Piccadilly, London, UK

5. Chromatographic NMR

Stefano Caldarelli

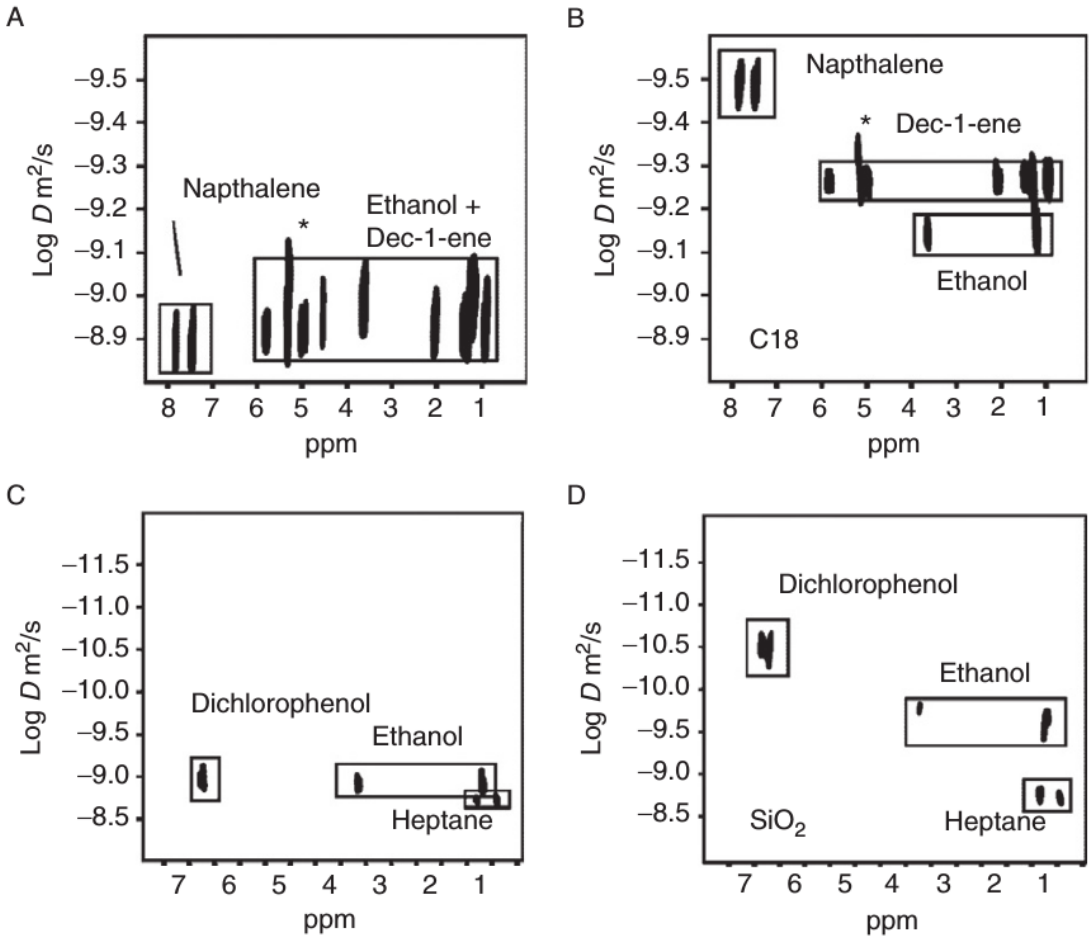

Figure 1 First chronological demonstration of the principle of chrom-NMR, on two pseudo-chromatographic setups. The top panels illustrate a DOSY layout for a mixture of naphthalene, ethanol and dec-1-ene in deuterated ethanol in pure solution (A) and upon addition of an ODS phase (B). A second set of DOSY experiments is shown in the bottom panels, for a mixture of dichlorophenol, ethanol and heptane in deuterated cyclohexane in pure solution (C) and upon addition of a bare porous silica phase (D). Adapted from Ref. 14. Copyright 2003 National Academy of Sciences, USA.

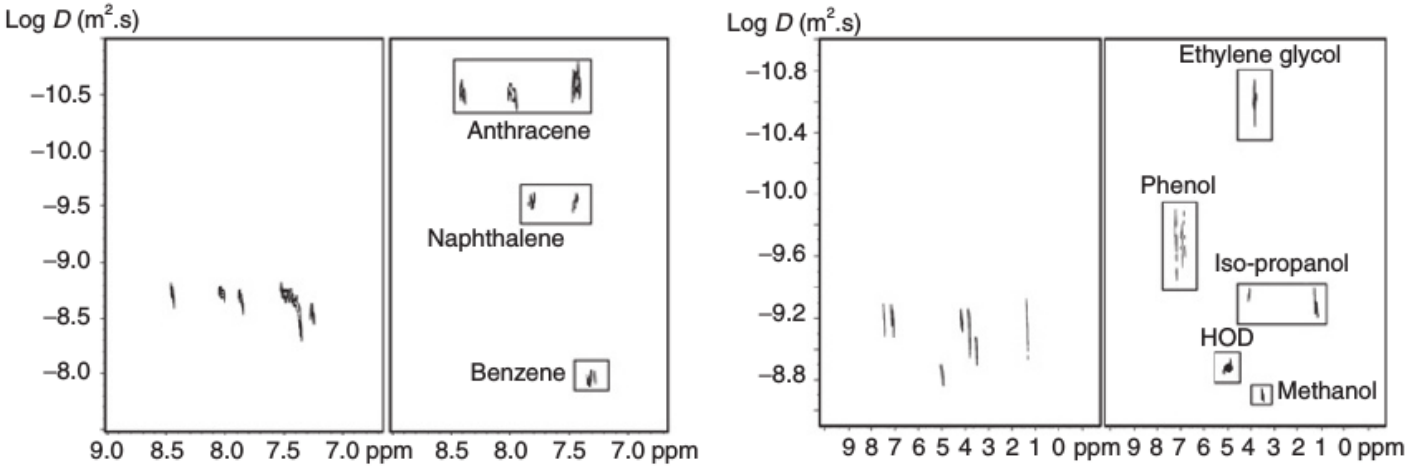

Figure 4 Example of the application of chrom-NMR/HRMAS with regular NMR solvents and bare silica as a solid phase. *Left panel*: aromatic molecule homologues in deuterated chloroform: benzene, naphthalene and anthracene. *Right panel*: alcohol mixture ethylene glycol, phenol, isopropanol in deuterated water. Adapted with permission from Ref. 53. Copyright 2008 Elsevier.

Nano Materials

Eur. Phys. J. B **31**, 545–551 (2003)
DOI: 10.1140/epjb/e2003-00064-0

THE EUROPEAN PHYSICAL JOURNAL B

Preparation and characterization of cobalt-based nanostructured materials

G. Carotenuto[1,a], L. Pasquini[2], E. Milella[1], M. Pentimalli[3], R. Lamanna[4], and L. Nicolais[1]

[1] Istituto per i Materiali Compositi e Biomedici. Consiglio Nazionale delle Ricerche. Piazzale Tecchio, 80 - 80125, Napoli, Italy
[2] Dipartimento di Fisica. Università di Bologna e INFM V.le Berti-Pichat 6/2I - 40127, Bologna, Italy
[3] MAT-COMP. ENEA C.R. Brindisi S.S. 7 Appia Km 713.7 - 72100, Brindisi, Italy
[4] BIOTEC-AGRO. ENEA C.R. Trisaia S.S. 106 Jonica Km 419.5 - 75026, Rotondella, Matera, Italy

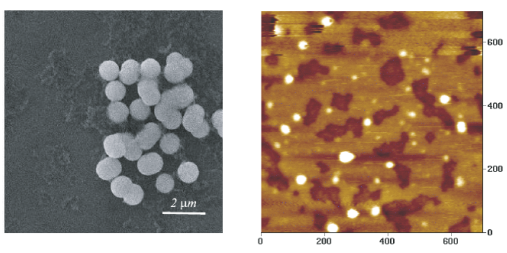

Fig. 1. (a) SEM-micrograph of micrometric cobalt particles and (b) AFM image showing the microstructure of a Co-$C_{12}H_{25}SH$ sample.

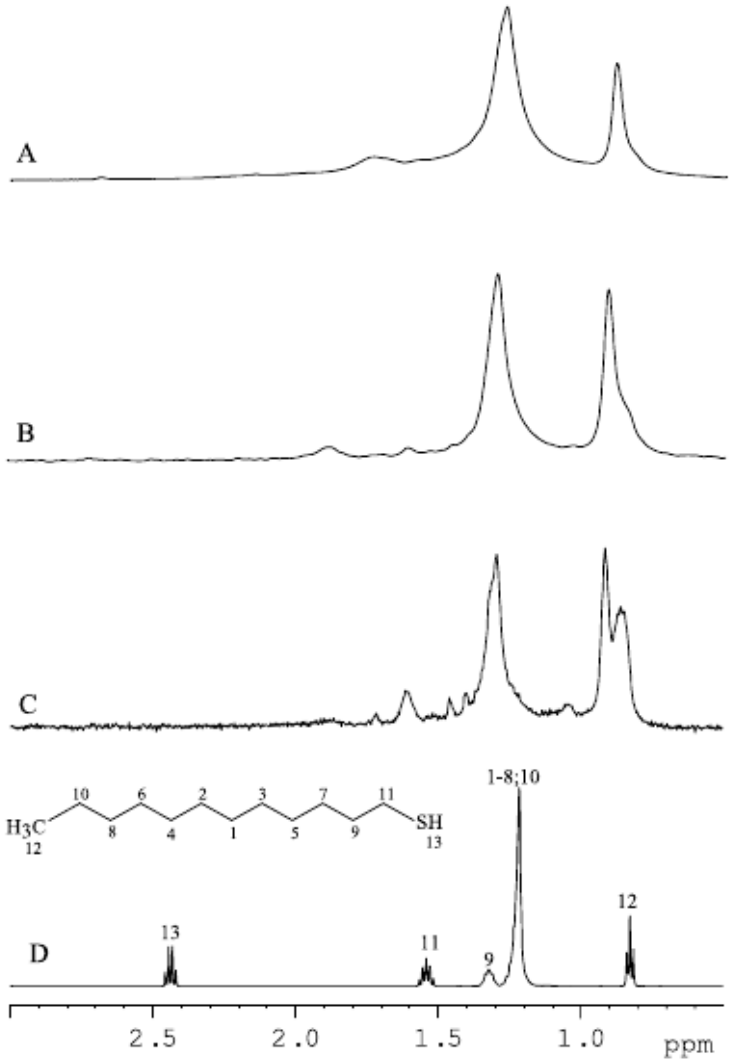

Fig. 6. ^{1}H HR-MAS NMR spectra in $CDCl_3$ of three different Co-$C_{12}H_{25}SH$ samples (A-C) and of pure $C_{12}H_{25}SH$ (D).

MgCl2 Ziegler-Natta Catalizers

J. Phys. Chem. C **2008,** *112,* 1081−1089 **1081**

Periodic DFT and High-Resolution Magic-Angle-Spinning (HR-MAS) ^{1}H NMR Investigation of the Active Surfaces of $MgCl_2$-Supported Ziegler−Natta Catalysts. The $MgCl_2$ Matrix

Vincenzo Busico,*,†,‡ Mauro Causà,† Roberta Cipullo,† Raffaele Credendino,† Francesco Cutillo,†,‡ Nic Friederichs,§ Raffaele Lamanna,∥ Annalaura Segre,⊥ and Valeria Van Axel Castelli†,‡,#

Dipartimento di Chimica, Università di Napoli Federico II, Via Cintia, 80126 Naples, Italy, Dutch Polymer Institute (DPI), P.O. Box 902, 5600 AX Eindhoven, The Netherlands, Sabic Europe, Research & Development, P.O. Box 319, 6160 AH Geleen, The Netherlands, ENEA, Centro Ricerche di Trisaia, 75026 Rotondella (MT), Italy, and Istituto di Metodologie Chimiche, CNR, P.O. Box 10, 00016 Monterotondo Stazione (RM), Italy

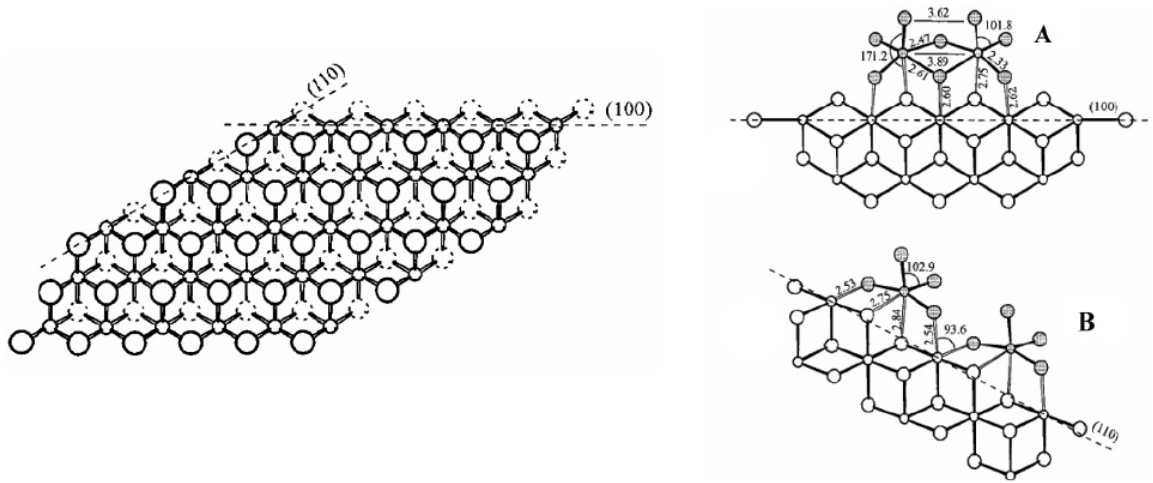

Figure 1. Models of $MgCl_2$ side edges and epitactic $TiCl_4$ surface adducts, according to refs 6 and 7 (adapted).

Octadecilmethyldimethoxysilane

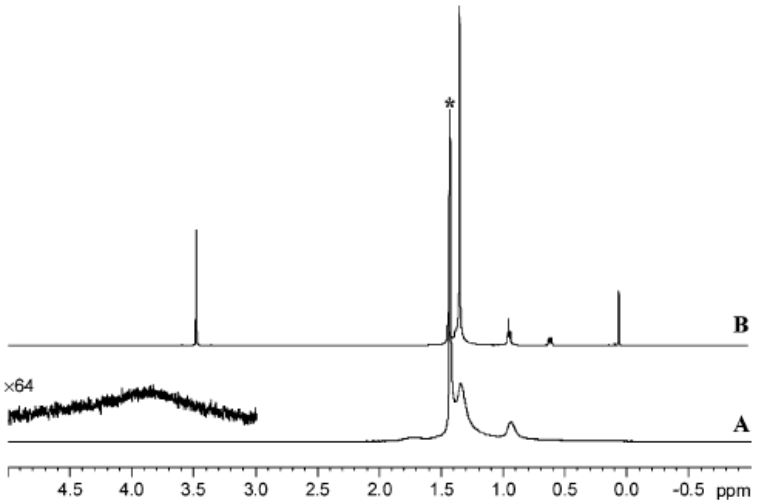

Figure 6. 600-MHz HR-MAS ^{1}H NMR spectra (at 30 ℃, 6 kHz spinning rate) of $MgCl_2$ suspended in cyclohexane-d_{12} solutions of octadecylmethyldimethoxysilane: $R_{Si/Mg}$ = (A) 0.4%, (B) 1.7%. The sharp peak marked with an asterisk is due to the residual protons of cyclohexane.

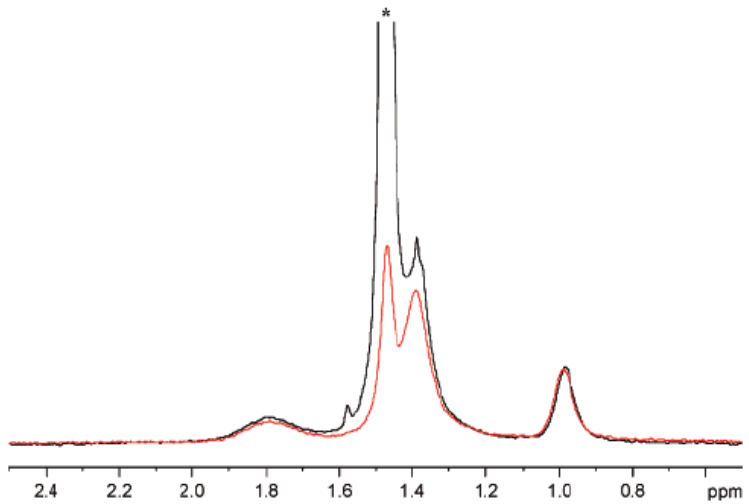

Figure 7. Diffusion-filtered 600-MHz HR-MAS ^{1}H NMR spectra (at 30 ℃, 6 kHz spinning rate, Δ = 100 ms) of the system presented in Figure 6A. Gradient intensities: black trace, 1.8 G cm^{-1}; red trace, 34.5 G cm^{-1}. The sharp peak marked with an asterisk is due to the residual protons of cyclohexane. The substantial invariance in the two experiments of the peak at δ = 0.94 ppm, due to the methyl protons of the octadecyl tail, is indicative of slow diffusion. Note, at the other extreme, the dramatic loss of intensity of the signal due to the solvent at high gradient intensity.

- La risonanza del OCH_3 é larga e spostata segno di forte legame con il $MgCl_2$.
- Il segnale dei CH_2 ha due componenti (Sharp 8 H) segno di un progressivo aumento di mobilita dei gruppi verso il metile finale.
- Per $R_{Si/Mg} > 0.7\%$ appare una fase mobile

  in scambio lento con la fase legata

Octadecilmethylmethoxysilane

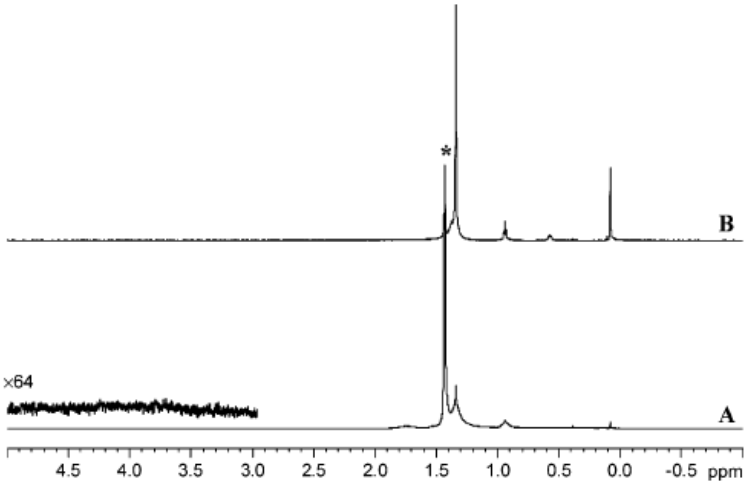

Figure 8. 600-MHz HR-MAS ^{1}H NMR spectra (at 30 ℃, 6 kHz spinning rate) of $MgCl_2$ suspended in cyclohexane-d_{12} solutions of octadecyldimethylmethoxysilane: $R_{Si/Mg}$ = (A) 0.2%, (B) 2.0%. The sharp peak marked with an asterisk is due to the residual protons of cyclohexane.

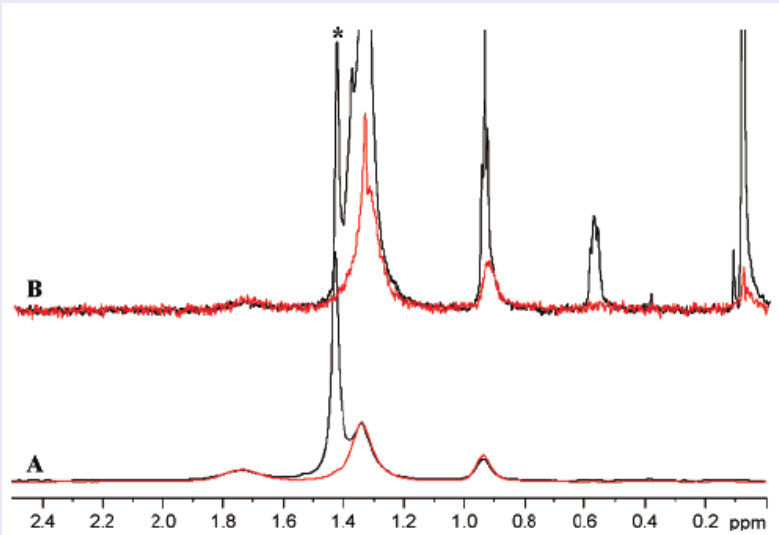

Figure 9. Diffusion-filtered 600-MHz HR-MAS ^{1}H NMR spectra (at 30 ℃, 6 kHz spinning rate, Δ = 100 ms) of the systems in Figure (A) 8A and (B) 8B. Gradient intensities: black trace, 1.8 G cm^{-1}; red trace, 34.5 G cm^{-1}. The sharp peak marked with an asterisk is due to the residual protons of cyclohexane.

- La soglia di saturazione é $R_{Si/Mg} > 3.3\%$ (appare il segnale OCH_3)
- Per $R_{Si/Mg} > 0.7\%$ appare una fase mobile in scambio lento con la fase legata
- La fase mobile non mostra il segnale del OCH_3 e quindi é in qualche modo legata alla superficie.

- La frazione di entrambi i silani fortemente legata é probabilmente associata con i piano 101 del $MgCl_2$.
- La frazione mobile del $RMeSi(OMe)$ é pobabilmente legata al piano 110 che contiene cationi Mg pentacoordinati che non riescono legare il $RMeSi(OMe)_2$ che é un elettrodonatore più debole.

Farina

Wheat Flour Enzymatic Amylolysis Monitored by in Situ ^{1}H NMR Spectroscopy

Maria E. Amato,[†] Giuliana Ansanelli,[‡] Salvatore Fisichella,[†] Raffaele Lamanna,[*,‡] Giuseppe Scarlata,[†] Anatoli P. Sobolev,[§] and Annalaura Segre[§]

Dipartimento di Scienze Chimiche, Università Viale A. Doria, 6-95125 Catania, Italy, CR ENEA Trisaia UTS Biotec-Agro, SS 106 Jonica Km 419.5, 75026 Rotondella (Mt), Italy, and Institute of Chemical Methodologies, CNR, M.B. 10, 00016 Monterotondo Stazione, Rome, Italy

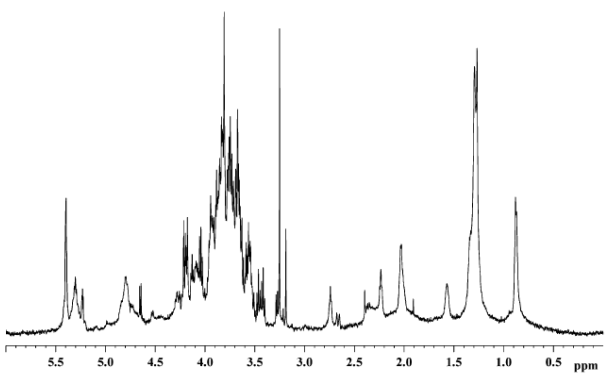

Figure 1. HR-MAS spectrum of a wheat flour sample in phosphate buffer, spun at 5 kHz.

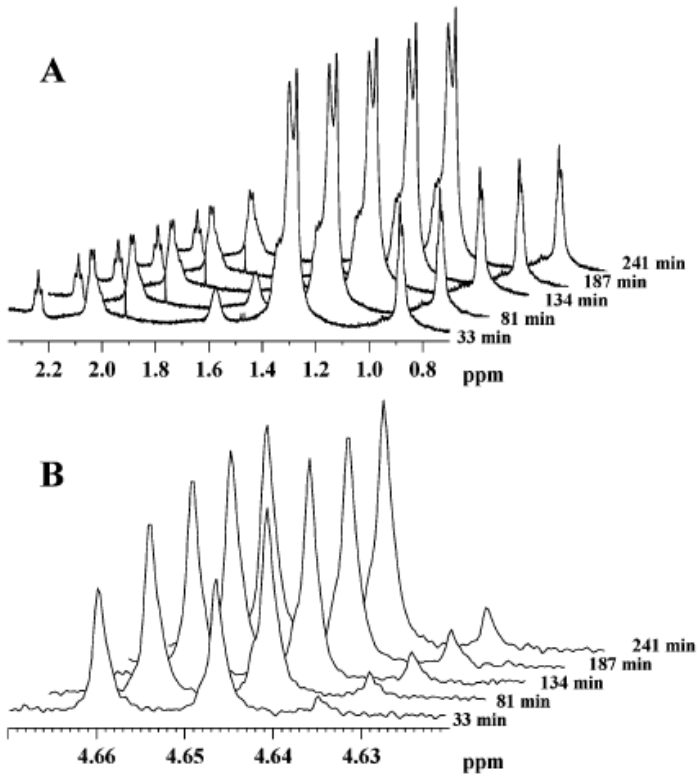

Figure 2. Stack plot of ^{1}H HR-MAS spectra of a wheat flour sample at different times of the enzymatic kinetic: (A) expansion of the region corresponding to the lipids, (B) expansion of the region corresponding to the β-glucose and β-maltose anomeric signals.

cinetiche

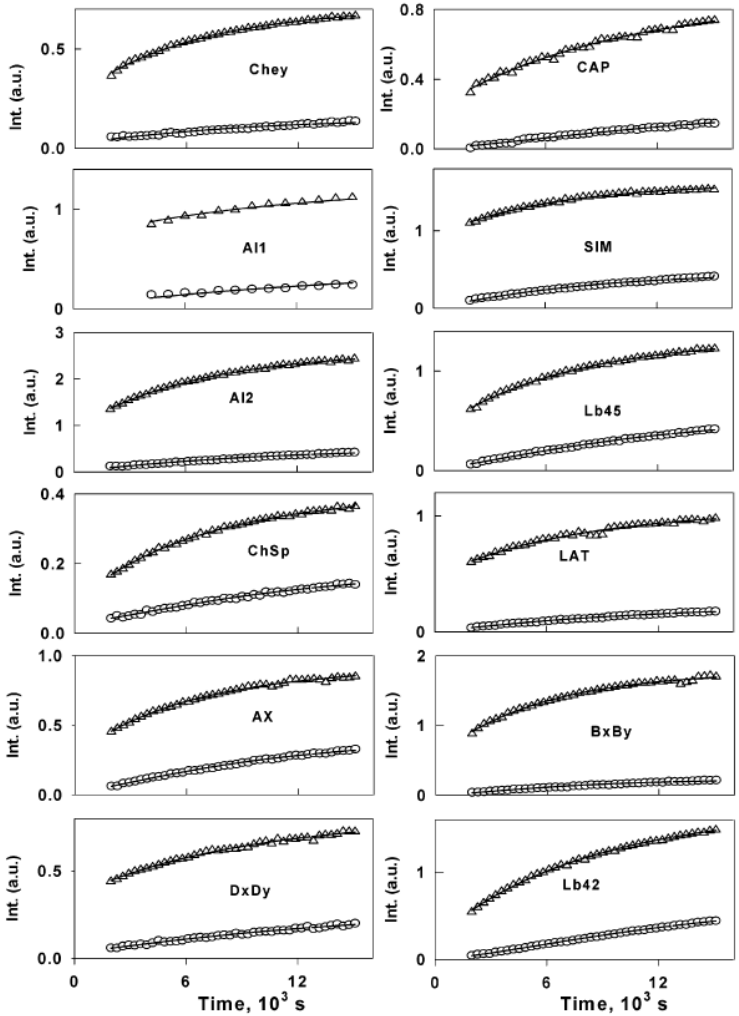

$$M(t) = \frac{V_{M_0} K_M}{V_{G_0}} - \left(\frac{V_{M_0} K_M}{V_{G_0}} - M_0\right) e^{-(V_{G0}/\alpha K_M)(1-e^{-\alpha t})}$$

$$G(t) = G_0 + \frac{V_{M_0}}{\alpha}(1 - e^{-\alpha t}) - \left(\frac{V_{M_0} K_M}{V_{G_0}} - M_0\right)(1 - e^{-(V_{G0}/\alpha K_M)(1-e^{-\alpha t})})$$

Figure 3. Intensities of the β-glucose (open circles) and β-maltose (open triangles) anomeric signals, as a function of time, for several wheat samples. The solid lines represent the best fit of data to eqs 1 and 2.

Coffee

HR-MAS ^{1}H NMR Study of Hydration Water in Arabica Green Coffee: Relation to the Final Beverage Quality

M. MIGLIETTA[1], R. LAMANNA[1], B. BONNLAENDER[2], L. NAVARINI[2], F. SUGGI LIVERANI[2], R. TOFFANIN[3,4]

[1]CR-ENEA Trisaia UTS BIOTEC-AGRO, SS 106 Jonica km 419.5, 75026 Rotondella, Italy
[2]Illycaffè SpA, Via Flavia 110, 34147 Trieste, Italy
[3]ARCHES, Castellana Grotte, Via G. Leuzzi 18, 70013 Castellana Grotte, Italy
[4]PROTOS Research Institute, P.O. Box 972, 34100 Trieste, Italy

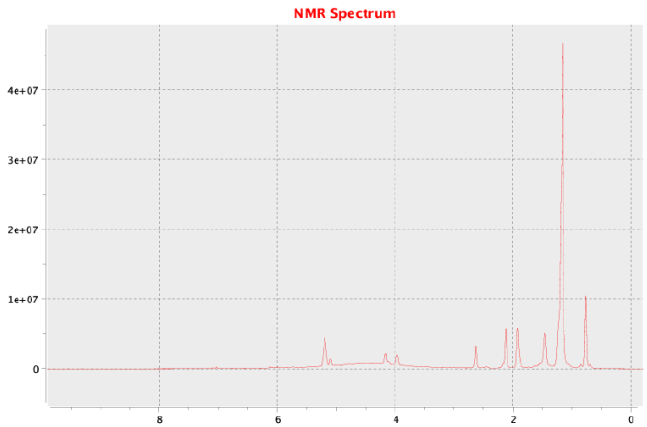

Figure 1. HR-MAS ^{1}H NMR spectrum of a powder sample of green coffee (*Coffea arabica*).

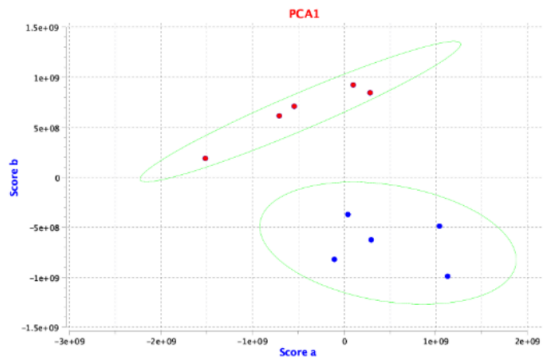

Figure 2. PCA scores plot produced from the NMR spectra of ten Arabica green coffee samples. Red circles represent good quality coffee whereas blue circles represent bad quality coffee.

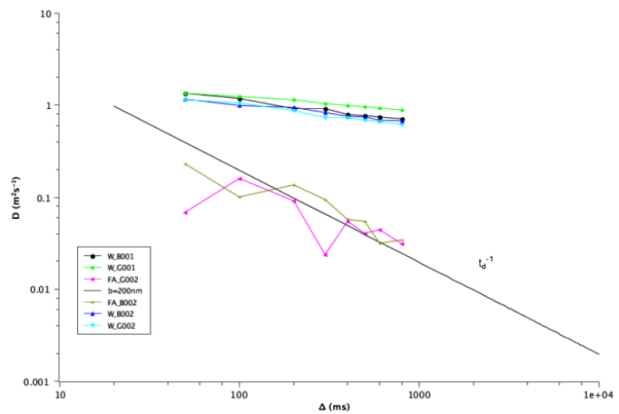

Figure 5. Diffusion coefficients of water (W) and fatty acids (FA) for selected Arabica green coffee samples as a function of the observation time (Δ). The restricted diffusion behaviour of fatty acids is reported for a barrier of 200 nm (solid line).

Royal jelly

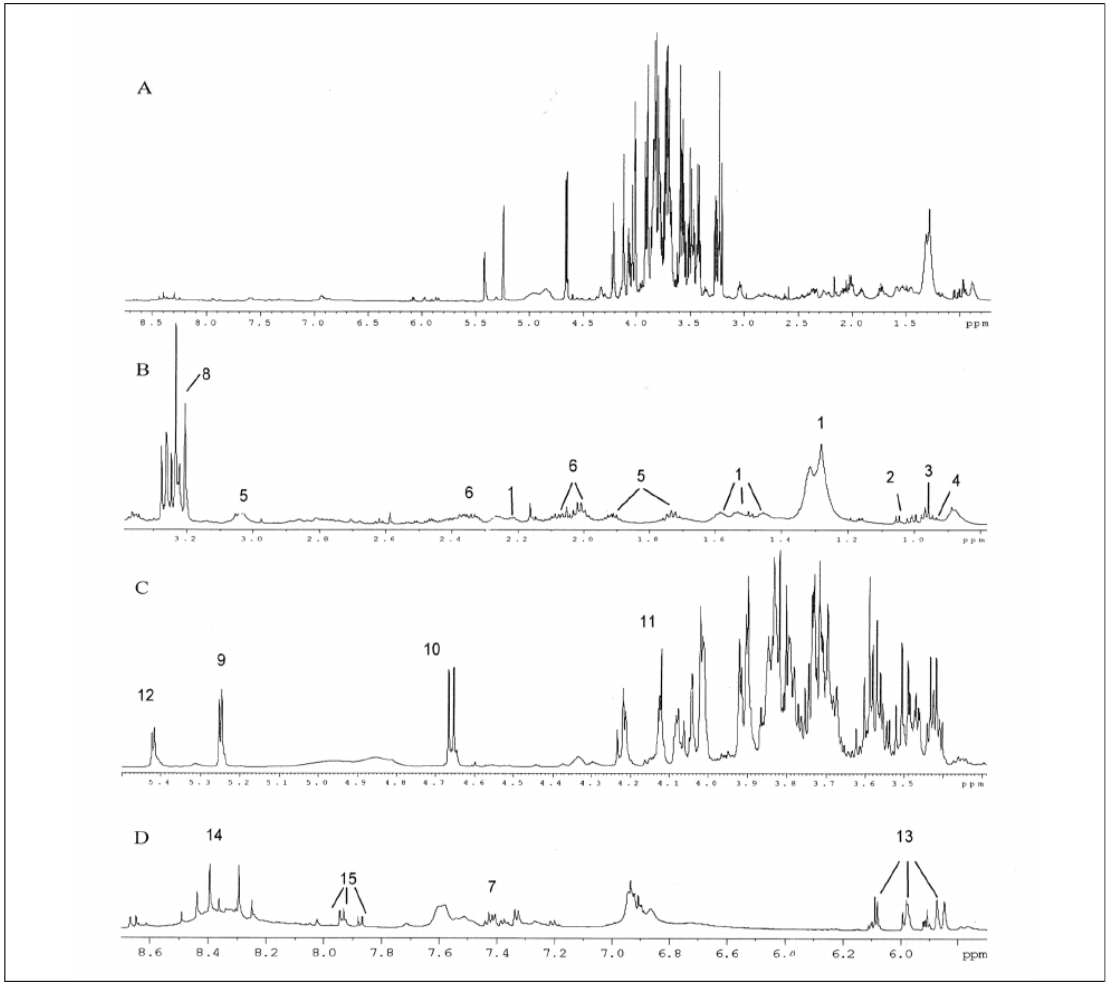

ORIGINAL RESEARCH ARTICLE

HR-MAS NMR metabolic profiling, furosine and (E)-10-Hydroxy-2-decenoic acid for qualitative and geographical discrimination of royal jelly

Maria Cristina Messia[1], Anatoli P Sobolev[2], Ana Maria Gómez-Caravaca[3], Raffaele Lamanna[4], Irene D'Amico[1], Maria Fiorenza Caboni[3], Emanuele Marconi[1*] and Luisa Mannina[2,5]

[1]DiAAA, Università degli Studi del Molise, Via De Sanctis, 86100 Campobasso, Italy.
[2]Istituto di Metodologie Chimiche, Laboratorio di Risonanza Magnetica "Annalaura Segre" CNR, 00015 Monterotondo, Rome, Italy.
[3]Dipartimento di Scienze degli Alimenti - Alma Mater Studiorum Università di Bologna, Piazza Goidanich, 60, 47521 Cesena (FC) Italy.
[4]CR ENEA Trisaia, UTS Biotech-Agro, I-75026 Rotondella (Mt), Italy.
[5]Dipartimento di Chimica e Tecnologie del Farmaco, Sapienza Università di Roma, Piazzale Aldo Moro 5, 00185 Rome, Italy.

Received 5 January 2012, accepted subject to revision 7 November 2012, accepted for publication 15 December 2012.

Fig. 1. 600.1 3 ^{1}H HRMAS (600 MH*z*) spectrum of: (A) a royal jelly sample; (B,C,D) expansion of some spectral regions with the assignment of some peaks is also reported: **1**, (CH_2)n of FA; **2**,VAL; **3**, LEU; **4**, ILE; **5**, LYS; **6**, PRO; **7**, PHE; **8**, CHN derivatives; **9**, α-GLC; **10**, β-GLC; **11**, FRU; **12**, SUC; **13**, RIB; **14**, GUA, ADE, INO spectral region; **15**, UR derivatives.

Origine geografica

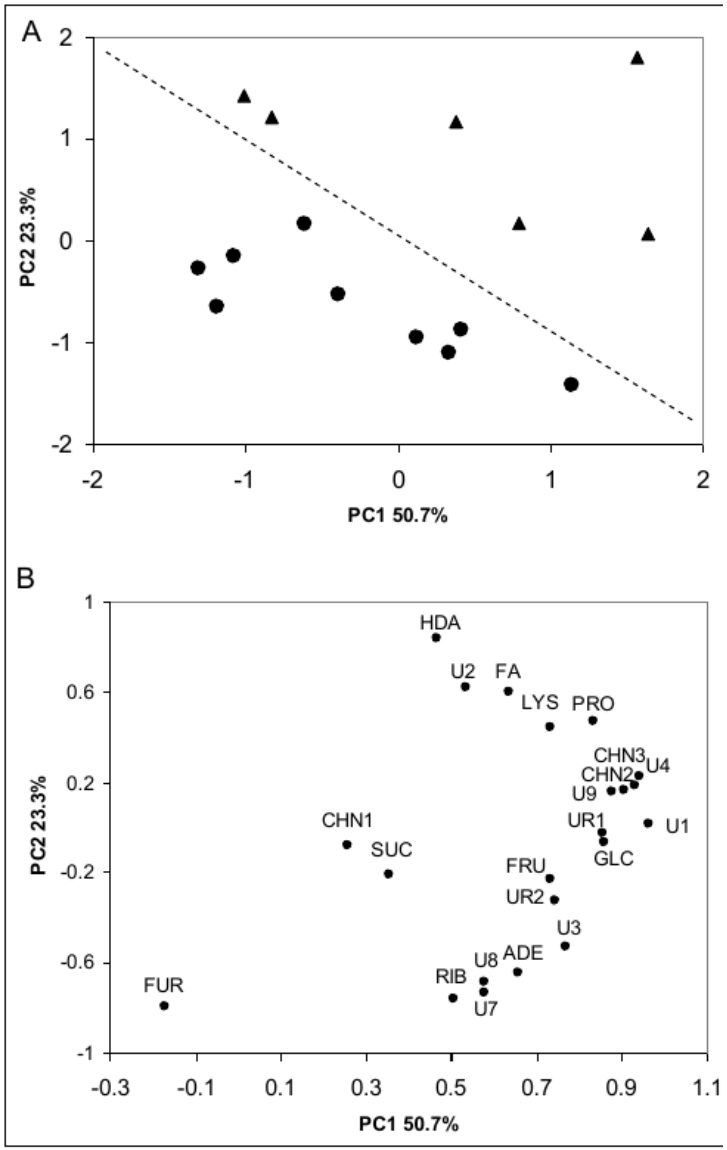

Fig. 3. Scores (A) and loadings (B) plots of PCA applied to the intensity of 22 selected variables. Chinese royal jelly samples (•), Italian royal jelly samples (▲).

Grazie !!